PERGAMON

Vision Research 39 (1999) 3351–3371

Vision Research

www.elsevier.com/locate/visres

# Short-range vernier acuity: interactions of temporal frequency, temporal phase, and stimulus polarity

Jonathan D. Victor *, Mary M. Conte

*Department of Neurology and Neuroscience, Weill Medical College of Cornell University, 1300 York Avenue, New York, NY 10021, USA*

Received 26 August 1998; received in revised form 4 January 1999

**Abstract**

We examined how vernier thresholds for flickering bars depend on the temporal frequency and relative temporal phase of the bars. The largest effect of relative phase (up to a fivefold increase in displacement thresholds) was seen at 2 Hz, and for most subjects. relative phase had little effect at 16 Hz and above. The effect of relative phase was essentially independent of contrast and trial duration. Thresholds were elevated by the greatest amount when bars were presented in antiphase, but at 1 and 4 Hz, quadrature phase offsets also led to substantial elevations in displacement thresholds. An experiment designed to examine the interaction of the vernier judgment with apparent motion failed to identify a role for mechanisms sensitive to apparent motion in threshold elevation. Another experiment in which the bars were modulated with sawtooth waveforms indicated that temporal correlation between the bars, rather than the ON versus OFF distinction, underlies the phase sensitivity. A simple dynamical model that posits partial rectification prior to a cross-correlation-like interaction accounts for the observed results. 

*Keywords:* Hyperacuity; Cross-correlation; ON and OFF subsystems

## 1. Introduction

Vernier alignment thresholds demonstrate the visual system's ability to make positional judgments substantially finer than the grain of the photoreceptor lattice (Westheimer, 1981; Klein & Levi, 1985), and is thus a classical example of 'hyperacuity'. In broad terms, much of the extensive body of hyperacuity literature considers two classes of models: local models, in which differences signaled by individual receptive fields or spatial filters (Klein & Levi, 1985; Wilson, 1986) support hyperacuity performance; and models whose performance is limited by noise at a second stage of processing, at which the position of the local filters is encoded (Burbeck, 1987; Morgan, Ward & Hole, 1990; Kooi, DeValois & Switkes, 1991; Levi & Waugh, 1996). These models are not mutually exclusive: for the same stimulus paradigm, a local model may hold for small spatial scales; while the two-stage model holds at larger spatial scales (Toet, van Eekhout, Simons, & Koenderink, 1987; Toet & Koenderink, 1988; Levi, Jiang, & Klein, 1990). Local models can indeed account for dependence of psychophysical thresholds on spatial aspects of the stimulus under conditions in which stimulus components are abutting or within a few minutes (Wilson, 1986). The presumptive association of model elements with cortical receptive fields is strengthened by the observations that the addition of flanking contours (Westheimer & Hauske, 1975; Levi, Klein, & Aitsebaomo, 1985) significantly raises vernier thresholds, but only within a few minutes' range. At short range, as predicted by local models, thresholds improve significantly as stimulus contrast increases (Morgan & Regan, 1987; Waugh & Levi, 1993a) and are dramatically affected by stimulus polarity (Mather & Morgan, 1986; Levi & Westheimer, 1987; O'Shea & Mitchell, 1990). With wider separations, vernier performance is relatively insensitive to stimulus contrast (Waugh & Levi, 1993c), polarity (Levi et al., 1990; O'Shea & Mitchell, 1990; Waugh & Levi, 1993c), asynchrony (Beard & Levi, 1997) or (for Gabor patches) spatial phase (Toet & Koenderink, 1988), orientation (Kooi et al., 1991),

* Corresponding author. Tel.: +1-212-746-2343; fax: +1-212-746-8984.

*E-mail address:* jdvicto@med.cornell.edu (J.D. Victor)

0042-6989/99/$ - see front matter 
PII: S0042-6989(99)00054-1

and spatial frequency (Kooi et al., 1991). This is to be expected from a two-stage model provided that positional uncertainty at the second stage is limiting.

In contrast to the wealth of information available concerning the dependence of hyperacuity performance on spatial factors, relatively little information is available concerning the role of temporal factors in hyperacuity tasks (Westheimer & Hauske, 1975; Westheimer & McKee, 1977; O'Shea & Mitchell, 1990; Waugh & Levi, 1993a,b,c; Wehrhahn & Westheimer, 1993; Fendick & Swindale, 1994). Under short-range conditions, presentation time has a substantial influence on thresholds, as expected from a single-layer local model, in which reduced presentation times would result in a proportional decrease in responses from local filters (Waugh & Levi, 1993a). With larger separations, presentation time is less important, as would be expected if performance is limited by noise in a positional encoding process (Waugh & Levi, 1993c). In a study of alignment of transiently-presented points, Wehrhahn and Westheimer (1993) found that temporal asynchronies of as little as 30 ms lead to elevation in threshold, but this work was restricted to the short-range regime. An analogous decrease in sensitivity to asynchrony was observed by Fendick and Swindale (1994), who studied the alignment of flicker-defined edges across a range of gap sizes.

Thus, in the local regime, temporal factors play a significant role in vernier acuity. The aim of this study is to examine the temporal factors underlying vernier acuity in sufficient detail so that inferences can be made concerning computational mechanisms. In contrast to previous studies (Westheimer & Hauske, 1975; Wehrhahn & Westheimer, 1993), we will use a frequency-domain approach, in which the components of a vernier target are modulated sinusoidally. One motivation for this approach is that linear processing of these signals preserves their sinusoidal nature, and the cross-correlation between two sinusoidal signals (of the same temporal frequency) depends sinusoidally on their relative phase.

Static presentation of two-bar vernier targets of like and opposite polarity can be thought of as the low-frequency limit of a frequency-domain analysis, in which the bars are presented in phase and in antiphase. Since vernier performance deteriorates for targets at opposite polarities, we expect a substantial phase-dependence of performance at low frequency (Mather & Morgan, 1986; Levi & Westheimer, 1987; O'Shea & Mitchell, 1990). However, experiments with static presentations do not lead to a clear prediction as to whether phase-dependence will persist to higher frequencies. Furthermore, the frequency-domain approach makes it natural to examine vernier performance in conditions intermediate between 'in phase' and antiphase, such as quadrature phase (0.25-cycle shifted) stimuli. These conditions are natural for analysis in the frequency domain, but have no immediate parallel for transient presentations. As will be seen below, performance under intermediate phase conditions is critically important for the qualitative understanding of the dynamics of vernier acuity.

## 2. Methods

### 2.1. Visual stimuli

Fig. 1 diagrams the typical vernier stimuli used in these experiments. The spatial layout consists of two horizontal bars, each 32 min long and 4 min wide. The ends of the bars were coincident with pixel boundaries, and contrast switched abruptly from 0 (background) to the full contrast of the bar along this axis. Along the width of the bars, we used a Gaussian profile (full width at half maximum set to 4 min), so that displacements of less than one pixel (1 min) could be realized (Krauskopf & Farell, 1991). Bar contrast was modulated sinusoidally in time. In all experiments, the modulation frequency of the two bars was the same, but (as illustrated in Fig. 1), they were not necessarily modulated in phase. Stimulus duration was 0.947 s unless otherwise noted, and masking was not used. Temporal profiles were ramped on and off over a period of 30 ms at the beginning and end of stimulus presentation. The choice of ramp duration was a compromise between the goal of avoiding sudden changes in stimulus contrast,

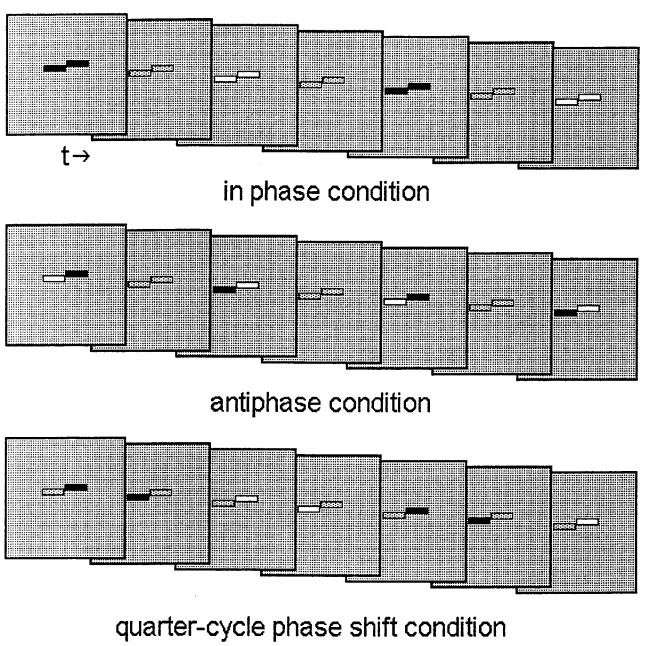


Fig. 1. A spatiotemporal diagram of the basic visual stimuli. Each frame represents a snapshot of the stimulus at quarter-cycle intervals. Bars were modulated sinusoidally in time, either in phase (upper sequence) or with a nonzero relative phase (middle and lower sequences).

and of maintaining the undistorted stimulus waveform for the duration of the nominal presentation. Since the stimulus transient amounts to an introduction of high temporal frequencies, the likely effect of an overly abrupt ramp would be to reduce observed temporal frequency-dependence, rather than to introduce a dependence artifactually.

These visual stimuli were produced on a Tektronix 608 display that subtended $4.4 \times 4.4°$ at a viewing distance of 114 cm and had a mean luminance of 150 cd/m$^2$. Control signals for the stimulator were produced by electronics modified from the design of Milkman, Schick, Rossetto, Ratliff, Shapley and Victor (1980) and interfaced to a DEC 11/73 computer. The electronics generated horizontal and vertical scan signals for a $256 \times 256$ pixel display at a frame rate of 270.3 Hz, and an intensity signal that was corrected (via a digital look-up table) for the nonlinear intensity/voltage relationship of the display oscilloscope.

### 2.2. Subjects and psychophysical methods

We used a two-alternative forced choice staircase procedure to determine contrast thresholds and displacement thresholds (71% correct). Trials were self-paced. For the determination of contrast thresholds, the stimuli shown in Fig. 1 were presented with the contrast of one of the bars randomly set to zero. The subject's task was to identify the location (left or right) of the bar at nonzero contrast. For the determination of displacement thresholds, the contrast of both bars was set to a predetermined multiple (e.g. $8 \times$) of the subject's detection threshold. The task was to identify which bar (randomly set to be the left or right bar) was displaced upward. For both detection and displacement measurements, the location of the stimuli was jittered up and down by 2 min from trial to trial, so that position of the individual bars was not available as a cue.

Staircases consisted of two preliminary reversals in which the parameter of interest was changed by 0.3 log units, followed by ten reversals with a step size of 0.1 log units. Completion of these staircases required approximately 55 responses. For each staircase a threshold estimate was obtained from the geometric mean of eight reversals: the final ten reversals with one high and one low outlier excluded. At each temporal frequency, estimates from four staircases were combined (geometric mean) to obtain each subject's contrast threshold. Staircases for each temporal frequency were presented in an interleaved manner, and the order of the staircases (e.g. high frequency first versus low frequency first) was counterbalanced within and across subjects. All subjects were given at least two practice staircases for each condition, with additional practice trials provided if performance did not appear to be stable. A similar protocol of practice trials, interleaving, and counterbalancing was used to obtain displacement thresholds from four to fourteen staircases for each condition. During the collection of displacement threshold data, occasional detection staircases were inserted to check for stability of detection thresholds. Additionally, there was some overlap of conditions across experiments, which served to check for reproducibility of displacement thresholds. Trials were organized into sessions of 16–24 staircases, lasting 1–2 h.

Studies were conducted in two male and eight female normal subjects (nine ranging in age from 18–44, one female aged 65). Two subjects (MC, RR) were experienced psychophysical observers and participated in all experiments. Additionally, at least three naive observers participated in each experiment. All had visual acuities (with correction if necessary) of 20/20 or better.

## 3. Results

### 3.1. Experiment 1: contrast and polarity

The first experiment investigates how displacement threshold depends on the relative phase of bars to be aligned. Each subject's displacement thresholds were determined for unmodulated bars ('0 Hz' in the figures) and bars modulated at 1, 4, and 16 Hz, at contrasts set equal to 2, 4, 8, and $16 \times$ the subject's detection threshold for each temporal frequency. Across subjects, these detection thresholds ranged from 0.015–0.064 for unmodulated bars, 0.021–0.104 at 1 Hz, 0.016–0.061 at 4 Hz and 0.031–0.175 at 16 Hz. Displacement thresholds from one subject (detection thresholds of 0.031 for unmodulated bars, 0.039 at 1 Hz, 0.029 at 4 Hz, and 0.060 at 16 Hz) are shown in Fig. 2. Across this range of frequencies, displacement thresholds were lower when the bars were in phase than when they were in antiphase. For unmodulated bars (Panel A), there was approximately a threefold difference between bars of the same luminance polarity and bars of opposite polarity. The thresholds differed by approximately a factor of 5 for bars modulated at 1 and 4 Hz, and by a factor of approximately 3 at 16 Hz. In all cases, displacement thresholds decreased somewhat with increasing contrast. Additionally, measurement of displacement threshold was most variable at the lowest contrast used ($2 \times$ detection threshold). However, there was little change in the displacement threshold ratio across an eightfold range of contrasts. Averages across subjects are shown in Fig. 3, and demonstrate essentially the same behavior. The largest antiphase to in phase threshold ratios were seen at 1 and 4 Hz. There was little if any dependence of the threshold ratio on contrast, even though there was a severalfold reduction in thresholds with increasing contrast, as reported by

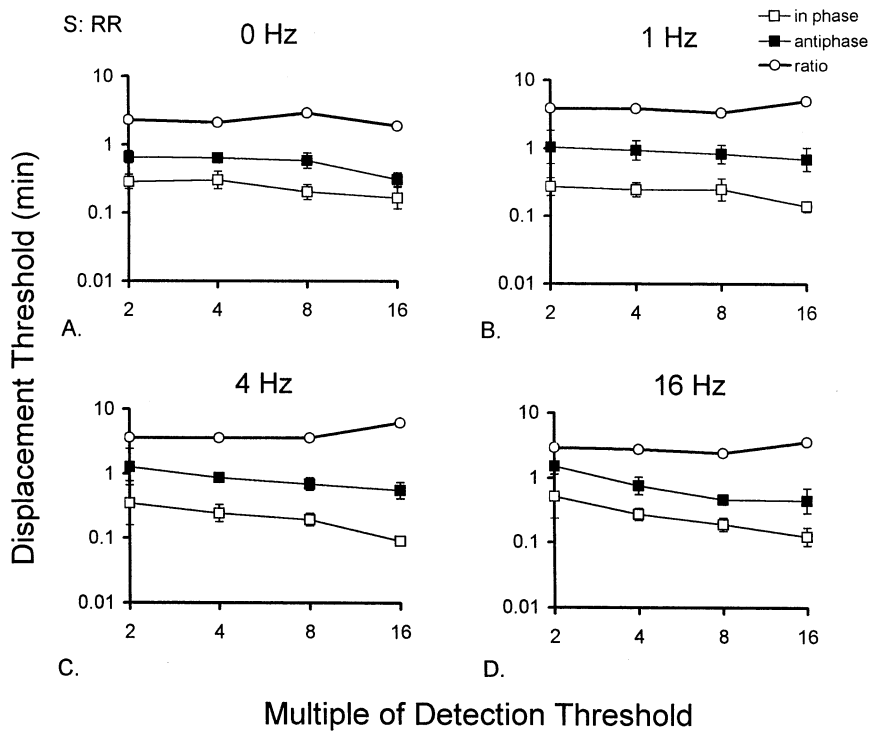


Fig. 2. Vernier thresholds for bars ($4 \times 32$ min) as a function of temporal frequency (panel), relative phase (open symbols: in phase. filled symbols: antiphase), and contrast (abscissae). Contrasts are given as a multiple ($2, 4, 8, 16 \times$) of the detection threshold, which was determined separately for each temporal frequency. At 0 Hz 'in phase' indicates bars with above-background luminance. 'antiphase' indicates bars with below-background luminance. At other temporal frequencies, bars were modulated sinusoidally. Stimulus duration: 0.947 s. Error bars represent $\pm 2$ S.E.M. as calculated from the replicate staircase runs for each condition. Subject RR.

other workers for in phase static stimuli (Wehrhahn & Westheimer, 1990; Krauskopf & Farell, 1991).

A more extensive look at the frequency-dependence of phase sensitivity is shown in Fig. 4. All thresholds were measured at $8 \times$ the detection threshold, since Figs. 2 and 3 show that there is little dependence of this ratio on contrast. The largest difference between in phase and antiphase displacement thresholds occurred at 2 Hz, both in individual subjects (seven of eight) and the group average. Phase sensitivity was still present at 16 Hz in some subjects (Panel A of Fig. 4, and Panel D of Fig. 2), but not in others (Panel B of Fig. 4). Across subjects, the antiphase versus in phase threshold ratio was minimally greater than 1 at 16 Hz, and not significantly greater than 1 at 20 or 24 Hz.

Flickering bars might be thought of as a rapid alternation between above-background bars and below-background bars. Conceivably, displacement thresholds for stimuli that involve below-background bars are substantially higher and as a consequence, thresholds for antiphase bars are elevated because two above-background bars are never simultaneously present. To rule out this possibility, we compared displacement thresholds for unmodulated bars above and below background. Across subjects, detection thresholds for the above-background bars (0.015–0.064, geometric mean 0.035) were somewhat higher than for below-background bars (0.017–0.032, geometric mean 0.025). Fig. 5 shows the comparison of above-background and below-background displacement thresholds for static bars in subject RR, using the detection threshold of the above-background bar as the base contrast. The above-background condition is the same as Panel A of Fig. 2, but the data were obtained from staircases run on separate days, and thus serve as a check on stability and reproducibility. The small increase in displacement thresholds for the below-background condition compared to the above-background condition was not statistically significant, and was not seen across subjects ($N = 6$). Thus, the notion that thresholds to antiphase bars are elevated because of markedly poor performance for one or the other polarity per se is ruled out.

### 3.2. Experiment 2: stimulus duration

In Experiment 1, trial duration was fixed at 0.947 s, so the number of oscillations of the stimulus and flicker frequency necessarily covaried. In Experiment 2, we decoupled these variables by varying trial duration. As shown in Fig. 6 (subject YLF) and Fig. 7 (the average across subjects), the phenomena we observed in Experiment 1 indeed represent a dependence on temporal frequency, rather than the number of temporal cycles in each trial. Trial duration was varied from one-quarter

of the standard duration (0.236 s) to twice the standard duration (1.894 s), so that the number of cycles of the 4 Hz stimulus varied from 1 to 8, and the number of cycles of the 16 Hz stimulus varied from 4 to 32. If the lack of a phase-dependence at high frequencies observed above reflected a ceiling phenomenon related to multiple stimulus presentations, then: (i) at any flicker frequency, the threshold ratio should become closer to 1 as stimulus duration increases; and (ii) across frequencies, threshold ratios should be similar if trials are equated for the number of cycles. How ever, as shown in Figs. 6 and 7, the ratio between antiphase and in phase thresholds increases, rather than decreases, as trial duration increases, contrary to (i). Furthermore, the ratio at 4 Hz is greater than the ratio at 16 Hz at all trial durations (statistically significant across subjects at $P < 0.05$ for durations of 0.47 and 1.89 s by paired $t$-test), contrary to (ii). Additionally, in the same five subjects (data not shown), there was no difference in performance at 1 Hz for trial durations of 0.95 versus 1.89 s. These observations rule out the possibility that trial duration, rather than temporal frequency, is responsible for the phenomena observed in Experiment 1.

### 3.3. Experiment 3: temporal phase in detail

The previous experiments only considered two relative phases, in phase and antiphase. We now examine the behavior of displacement thresholds for intermediate phases, in steps of 0.125 cycle. Data from one subject (RR) is shown in Fig. 8. At 1 Hz, there is a gradual increase in displacement threshold as relative phase increases from 0 (in phase) to 0.5 cycle (antiphase). At 4 Hz there is a stronger dependence on relative phase, and the data suggest that most of the effect of phase is seen as relative phase varies from 0 to 0.25 cycle. At 16 Hz, as expected from Experiment 1, relative phase has less of an effect, and could not be discerned in all subjects (see Fig. 9). But in this subject, a pattern of dependence on relative phase similar to that seen at 4 Hz could be identified: thresholds obtained with intermediate relative phases (0.125, 0.25, and 0.375 cycle) are closer to thresholds in the antiphase condition than in the in phase condition.

The average behavior across subjects is shown in Fig. 9. We have normalized each displacement threshold by dividing it by the subject's threshold obtained in the in phase condition (at the same temporal frequency) prior

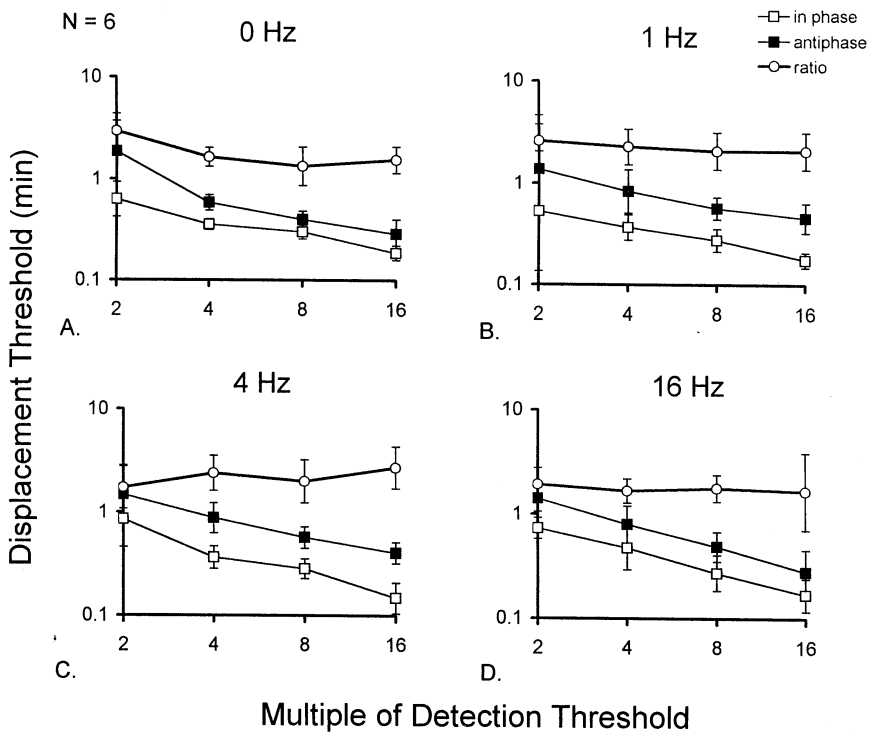


Fig. 3. Cross-subject averages of vernier thresholds for bars as a function of temporal frequency, relative phase. and contrast (abscissae). For thresholds in the in phase and antiphase conditions, error bars represent $\pm 2$ S.E.M., calculated from the average threshold for each subject. For the threshold ratio, error bars represent $\pm 2$ S.E.M. of the threshold ratios calculated from the two condition-averages within each subject. All data points represent averages across six subjects, except for those marked with triangular symbols. At 1 Hz, the average includes five subjects at $2\times$ threshold and four subjects at $16\times$ threshold. At 16 Hz, the average includes four subjects at $2\times$ threshold, five subjects at $8\times$ threshold, and three subjects at $16\times$ threshold. Other details as in Fig. 2.

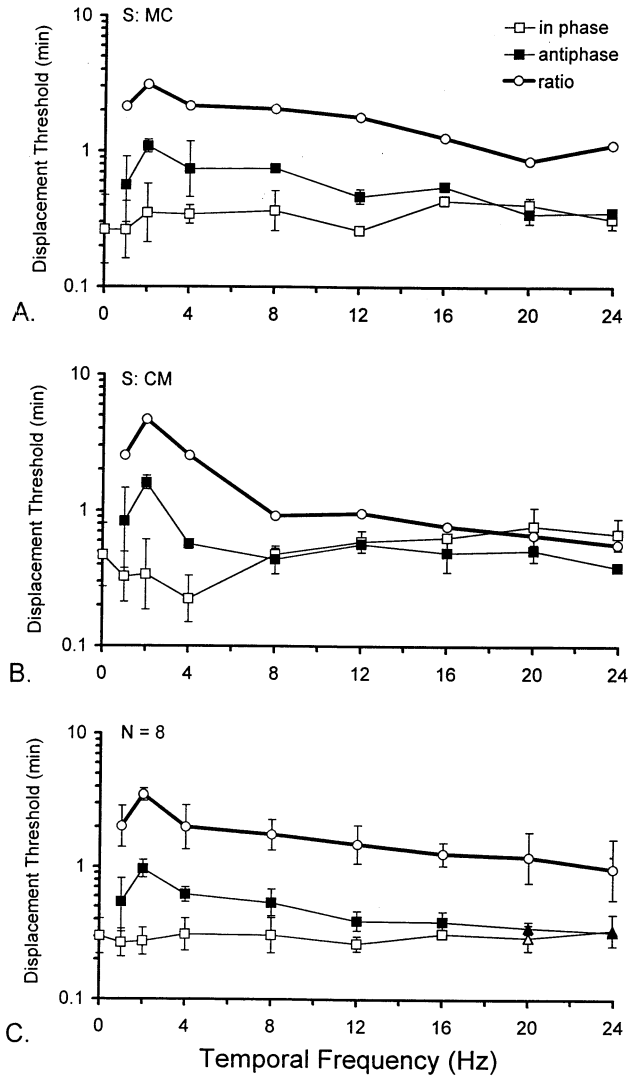


Fig. 4. Vernier thresholds as a function of temporal frequency (abscissae) and relative phase. Contrast was set to 8 × detection threshold, determined separately for each temporal frequency. Other details as in Fig. 2. Panel A: Subject MC. Panel B: Subject CM. Panel C: Average across all subjects. Error bars represent ±2 S.E.M. as calculated across subjects, as in Fig. 3. At 16 Hz and below, the average included eight subjects; at 20 Hz, six subjects; at 24 Hz, five subjects.

to averaging. At 1 Hz, there is a gradual increase in displacement threshold with increasing relative phase. At 4 Hz, thresholds for relative phases of 0.25, 0.375, and 0.5 cycle are not significantly different from each other ($P < 0.05$ by paired $t$-test), but are significantly elevated in comparison to thresholds for relative phases of 0 and 0.125 cycle ($P < 0.05$ by paired $t$-test). Note that the error bars in Fig. 9 reflect the range of variation across subjects. Within each subject, the pattern of threshold elevation was sufficiently consistent so that the above *paired* comparisons reached statistical significance. At 16 Hz, there is not enough of a systematic phase-dependence across all subjects (consistent with Panel D of Fig. 3, and Panel C of Fig. 4) to discern the effect of the intermediate phase shifts.

### 3.4. Experiment 4: possible role of apparent motion

The unexpectedly large effect of a quarter-cycle phase shift (Experiment 3, Fig. 9B) suggested the possibility that mechanisms subserving motion detection, which are optimally driven by quarter-cycle phase shifts (Nakayama & Silverman, 1985), might be involved in the threshold elevations we observed. This possibility was investigated directly by the experiment diagrammed in Fig. 10. The spatial configuration was modified to consist of three bars, with the two flanking bars fixed in alignment and the central bar at a variable vertical displacement. The three bars were modulated sinusoidally, with the phases of the flanking bars shifted with respect to that of the central bar. In one configuration, here called 'no apparent motion', the flanking bars were modulated in synchrony, both at the same phase lag with respect to the central bar. In the 'apparent motion' configuration, the flanking bars were modulated asynchronously, one with a phase lead with respect to the central bar, and one with a phase lag with respect to the center. In this configuration, the phases of the three bars were staggered, and provided a strong percept of apparent motion, from the flanking bar in phase lead to the flanking bar in phase lag. No such percept of apparent motion was present in the first configuration, even though the absolute phase shift between the center bar and each of the flanking bars was identical. Note that for phase shifts of 0 and 0.5, the two stimuli are identical to each other.

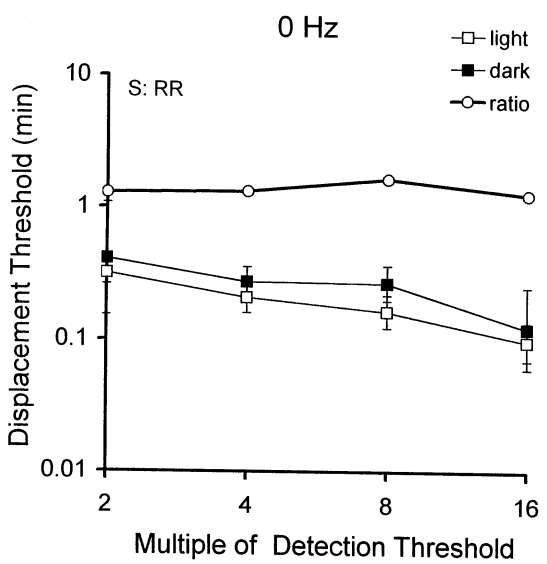


Fig. 5. Vernier thresholds for unmodulated bars as a function of polarity and contrast (abscissa). Contrast values are given as a multiple of the detection threshold for above-background bars. Other details as in Fig. 2. Subject RR.

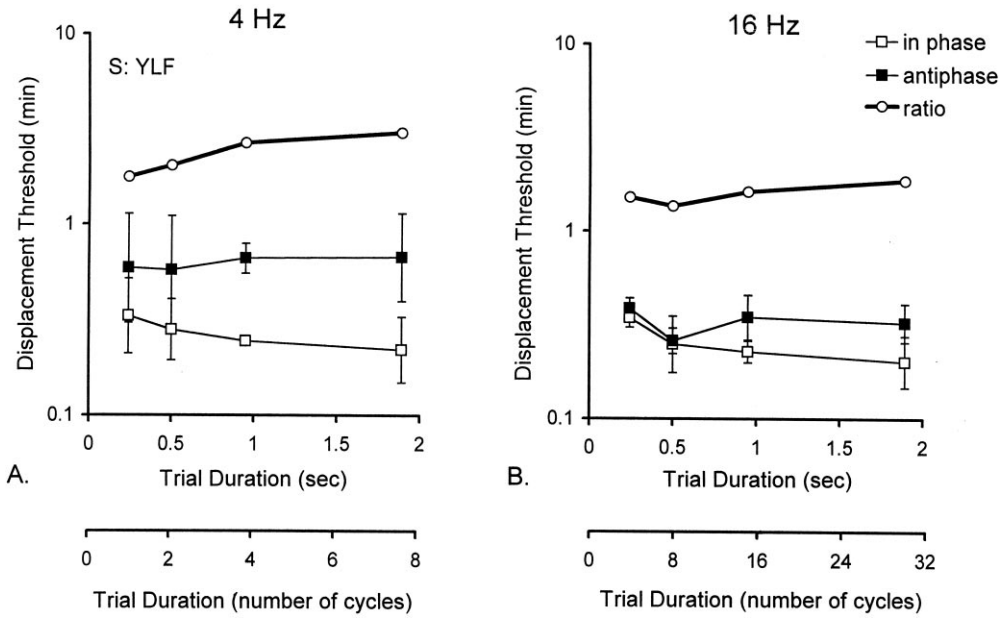


Fig. 6. Vernier thresholds as a function of temporal frequency (panel), relative phase (open symbols: in phase, filled symbols: antiphase), and trial duration (abscissae). Contrast was set to 8 × detection threshold, determined separately for each frequency and a presentation time of 0.947 s. Other details as in Fig. 2. Subject YLF.

The behavior of displacement thresholds as a function of temporal frequency and the spatial configuration of the phase shifts is shown in Fig. 11. As in the two-bar experiments, the largest effect of temporal phase shift is seen at 2 Hz (mean threshold of 0.19 min in phase, 0.68 min out of phase), and there was comparatively little effect of temporal phase shift at 16 Hz (mean threshold of 0.18 min in phase, 0.34 min out of phase). At all temporal frequencies, there was no difference between the thresholds obtained when the phases of the three bars were configured to minimize the percept of apparent motion, compared to a configuration with a strong percept of apparent motion.

### 3.5. Experiment 5: sawtooth waveforms

Krauskopf (1980) examined detection of luminance changes driven by periodic temporal waveforms consisting of a rapid transient in one direction, followed by a gradual return (sawtooth waveforms). He found that thresholds for detection of up-transient fluctuations were elevated by adaptation to an up-transient waveform, that thresholds for detection of down-transient fluctuations were elevated by adaptation to a down-transient waveform, and that there was little cross-adaptation. We used this approach to examine the role of the ON–OFF dichotomy in the phase-dependence of displacement thresholds.

We used the spatial configuration of Fig. 1. The sinusoidal temporal modulation signals were replaced by sawtooth waveforms centered about the mean luminance at frequencies of 1 Hz (Krauskopf, 1980), 2 and 4 Hz. At 8 Hz and above, the up-transient sawtooth and the down-transient sawtooth waveforms appeared indistinguishable. At each temporal frequency, there are three ways of assigning sawtooth waveforms: both bars driven by an up-transient sawtooth, denoted 'UU', both bars driven by a down-transient sawtooth, denoted 'DD', and one bar driven by an up-transient sawtooth, while the other bar is driven by a down-transient sawtooth, denoted 'UD'. In one subject, we verified that reversing or randomizing the assignments did not affect displacement thresholds. For each of these assignments, the waveforms were presented either with their transients synchronous ('in phase'), or their transients separated by half a modulation cycle ('antiphase'). These six possibilities are diagrammed in Fig. 12. In the UU and DD configurations, in phase presentation maximizes the cross-correlation between the temporal signals driving the two bars, while the antiphase presentation results in a negative cross-correlation. In the UD configuration, in phase presentation results in anticorrelated signals, but the antiphase condition results in positively correlated signals. That is, if temporal correlation governed displacement threshold, there would be a reversal of the effect of phase in the UD configuration. On the other hand, if low thresholds required simultaneous presence of signals from both bars within either the ON or the OFF pathway, thresholds should be low for the UU and DD conditions and high for the UD condition, independent of the phase of the transient. In short, the UD configuration allows us to distinguish between the role of stimulus polarity (i.e. ON versus OFF) and degree of cross-correlation.

Displacement thresholds were measured at 16 × each subject's mean detection threshold for up-transient and down-transient stimuli. There was no significant difference between these thresholds. Results for one subject (CM) are shown in Fig. 13. As expected, in the configurations in which both bars were driven by the same sawtooth waveform (UU and DD), thresholds were significantly higher in the antiphase condition than in the in phase condition. However, in the UD condition, the antiphase displacement threshold was lower than the in phase displacement threshold at all frequencies, with a statistically significant difference at 1 Hz.

Across all subjects (Fig. 14), the same pattern was seen. In particular, all subjects showed an increased displacement threshold in the antiphase UU and DD conditions compared to the in phase UU and DD conditions ($P < 0.0001$ at 1, 2, and 4 Hz by one-tailed paired $t$-test), but a reversal of this phase-dependence in the UD configuration ($P < 0.01$ at 1 Hz, $P < 0.05$ at 2 and 4 Hz). That is, with transients of opposite (ON versus OFF) polarity, the 'advantage' of in phase stimulation over antiphase stimulation is reversed. The displacement threshold is lower in the antiphase condition, which maximizes the temporal cross-correlation. Furthermore, thresholds in the antiphase UD condition were lower than thresholds in the antiphase UU or DD conditions ($P < 0.01$ at 1, 2, and 4 Hz). That is, the elevation in threshold seen with antiphase transients of the same (ON or OFF) polarity can be reversed by a configuration in which the polarities are opposite. Together, these observations show that separate stimulation of the ON and the OFF pathways by the sawtooth-modulated bars is not the main factor that determines displacement threshold: bar polarity and the relative phase of the transients interact in a manner consistent with the notion that thresholds are lowest when cross-correlation is maximized.

## 4. Discussion

### 4.1. Summary of results

Our analysis of the effects of temporal frequency and relative temporal phase on vernier displacement thresholds extend the well-known findings that for static or low-temporal-frequency stimuli, targets with opposite-polarity components are associated with higher thresholds (e.g. Mather & Morgan, 1986; O'Shea & Mitchell, 1990; Wehrhahn & Westheimer, 1993; Levi & Waugh, 1996; Beard & Levi, 1997). Experiment 1 (Figs. 2–4) showed that displacement thresholds are increased when the stimulus components are in antiphase, by a factor of 3 or more. The frequency range in which the threshold elevation is maximal is 1–4 Hz. The largest threshold elevation occurs at 2 Hz, and at sufficiently high frequencies (16 Hz in some subjects, 24 Hz in all), relative phase has no effect. The effects of phase and frequency are essentially independent of contrast, for contrasts from 2 to 16 × detection threshold. The results of Fig. 5 rule out the possibility that the 'relative phase' effect was really due to different displacement thresholds for above-background and below-background bars. The results of Experiment 2 (Figs. 6 and 7) rule out the possibility that the observed dependence on temporal frequency really reflect a dependence on the number of cycles presented.

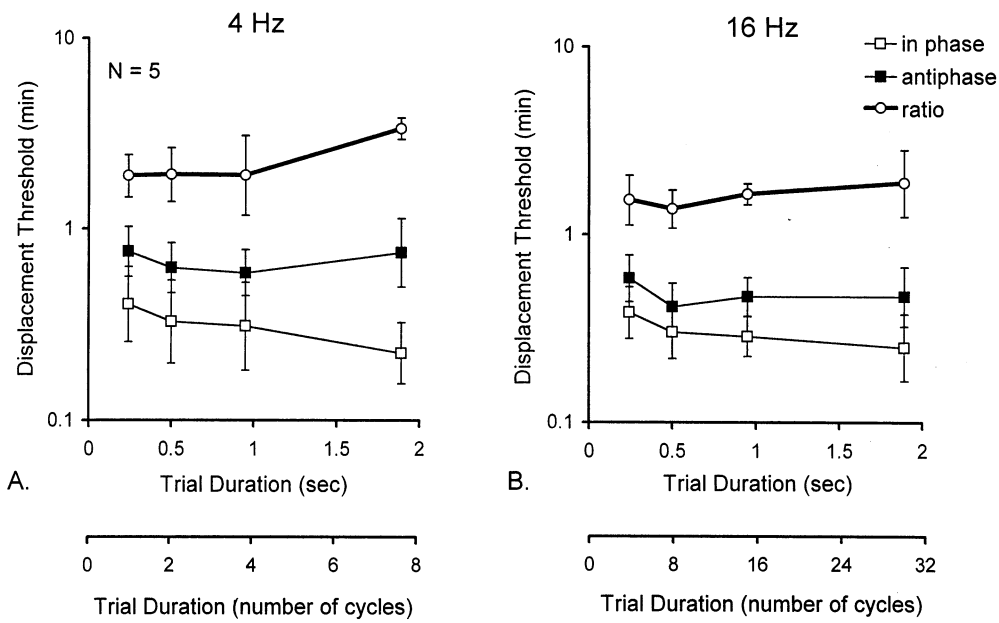


Fig. 7. Cross-subject averages of vernier thresholds as a function of temporal frequency, relative phase. and trial duration. Each data point represents an average of five subjects. Error bars represent ±2 S.E.M. as calculated across subjects, as in Fig. 3. Other details as in Fig. 6.

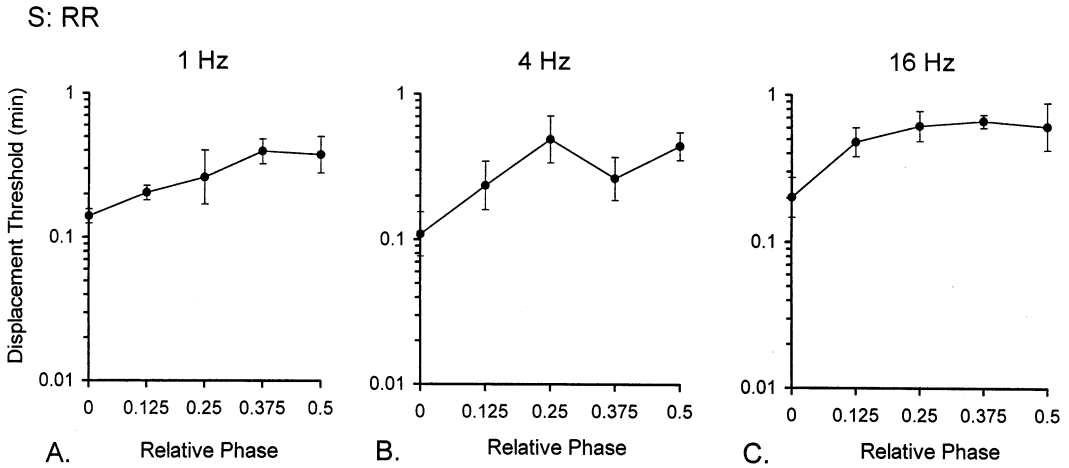


Fig. 8. Vernier thresholds as a function of temporal frequency (panel) and relative phase (in cycles, abscissae). Contrast was set to 16 × detection threshold, determined separately for each frequency. Other details as in Fig. 2. Subject RR.

The other experiments were designed to constrain possible models for these findings. Experiment 3 (Figs. 8 and 9) shows that at 1 and 4 Hz, it is not necessary for the stimuli to be in antiphase in order to have significant threshold elevations. The quadrature condition is expected to make the apparent motion percept the strongest (Nakayama & Silverman, 1985), but Experiment 4 (Fig. 11) shows that this is not related to the extent of threshold elevation. Finally, Experiment 5 (Figs. 13 and 14) indicates that the effects of relative phase are not a consequence of the ON versus OFF dichotomy, as elaborated below.

### 4.2. A model framework

To understand the kinds of computations that could account for our findings, we consider a general model framework (Fig. 15) in which signals from each of the two bars, denoted $S_A(t)$ and $S_B(t)$, are processed independently, and these signals are then combined. The separate processing stage may contain both linear and nonlinear components, and the combination stage may also contain both linear and nonlinear components. As a minimal model for the separate-processing stage, we postulate an initial linear filter $L_S$ followed by a nonlinearity $N_S$. Following this local nonlinear process, signals $X_A(t)$ and $X_B(t)$ may then be further filtered prior to their combination. This filtering might occur both at the local processing stage, diagrammed as $L_1$, and at the combination stage prior to combination of signals, diagrammed as $L_2$. We denote the output of $L_2$ by the signals $Y_A(t)$ and $Y_B(t)$. Finally, there is a combination process $N_C$ at which signals $Y_A(t)$ and $Y_B(t)$ are combined, and produce an output $Z(t)$ that represents some measure of the similarity of $Y_A(t)$ and $Y_B(t)$. $N_C$ may be thought of as cross-correlation, but its precise functional form is not assumed to be multiplication. For example, we could also assume that $Z(t)$ can only be nonzero if both inputs are simultaneously positive. Psychophysical sensitivity (i.e. the reciprocal of the displacement threshold) is assumed to be monotonically related to $Z_{mean} = \langle Z(t) \rangle$, the average of $Z(t)$ over time.

Our model is intended to be an abstraction of the computations underlying hyperacuity, rather than a model whose components correspond in a detailed fashion to specific neurons. At a minimum, each 'linear' stage of the model likely corresponds to a concatenation of transformations by several physiologic processes (e.g. $L_S$ could include phototransduction and filtering at outer and inner plexiform layers). The framework of Fig. 15 is also a caricature in the sense that a full account of the computations underlying hyperacuity judgments might well require several pathways of this sort, to process stimuli of a range of sizes or eccentricities (Levi & Klein, 1990; Whitaker, Mäkelä, Rovamo, & Latham, 1992; Whitaker, Rovamo, Macveigh & Mäkelä, 1992). The purpose of the model is to indicate what functional processing stages are relevant to phase- and frequency sensitivity, and to constrain their qualitative features, rather than to provide an exact fit to our data.

To begin to analyze how the components of the model shape its predictions, we assume that the combination process $N_C$ is strictly multiplicative. (Below we will see that other choices for $N_C$ do not substantially influence the model's key predictions). In all of our experiments, the input signals $S_A(t)$ and $S_B(t)$ share a common period, so therefore the two signals $Y_A(t)$ and $Y_B(t)$ that arrive at $N_C$ are also periodic with this period. We denote the common period by $P$, and their common fundamental frequency by $f_0 = 1/P$. We can compute the cross-correlation of $Y_A(t)$ and $Y_B(t)$ (i.e. the average value of their product) in the frequency

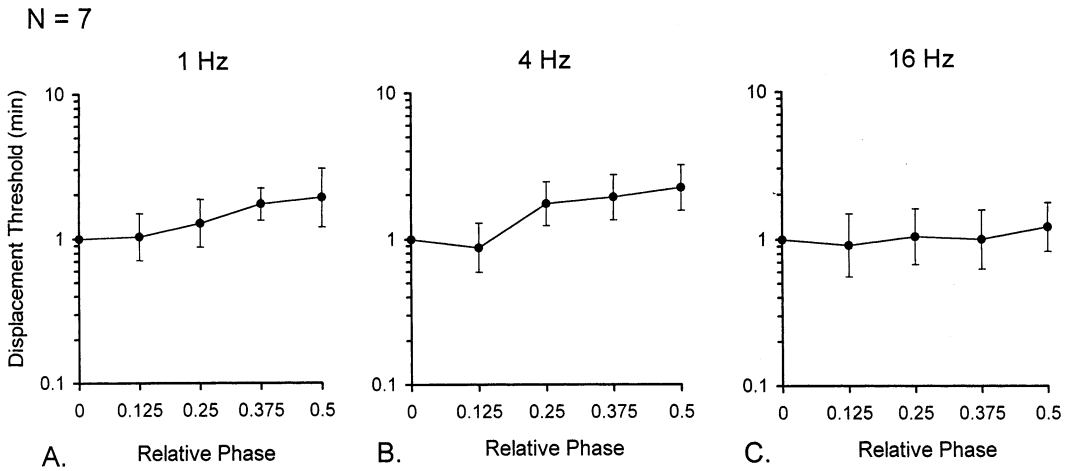


Fig. 9. Cross-subject averages of vernier thresholds as a function of temporal frequency and relative phase. Prior to averaging, thresholds for each subject are normalized by the threshold measured at a relative phase of 0. Each data point represents an average of seven subjects. Error bars represent $\pm 2$ S.E.M. as calculated across subjects. Other details as in Fig. 8.

domain as well as in the time domain. Because sinusoids at distinct harmonics of the inputs are orthogonal, the only nonzero contributions result from the products of the Fourier coefficients of $Y_A(t)$ and $Y_B(t)$ at corresponding frequencies. That is,

$$\langle Z(t)\rangle = \sum_{n=-\infty}^{\infty} \tilde{Y}_A(nf_0)\ \tilde{Y}_B(-nf_0), \tag{1}$$

where $\tilde{Y}_A(nf_0)$ and $\tilde{Y}_B(nf_0)$ are the Fourier coefficients of $Y_A(t)$ and $Y_B(t)$ at the $n$th harmonic of the fundamental frequency $f_0$:

$$\tilde{Y}_A(f) = \frac{1}{P}\int_0^P Y_A(t)\exp(-2\imath\pi ft)dt, \tag{2}$$

and similarly for $\tilde{Y}_B(f)$.

Since distinct harmonics of $Y_A(t)$ and $Y_B(t)$ do not interact, it is helpful to focus on the special case in which each of these signals is a sinusoid at the $k$th harmonic of the stimulus (i.e. at the frequency $kf_0$, for $k \neq 0$). We require equal amplitudes but allow for separate phase shifts, so that $Y_A(t) = Y\cos[2\pi kf_0t + \phi_A(kf_0)]$, and $Y_B(t) = Y\cos[2\pi kf_0t + \phi_B(kf_0)]$. For this choice of $Y_A(t)$, $\tilde{Y}_A(nf_0)$ is nonzero only for $n = \pm k$; at these values, Eq. (2) shows that $\tilde{Y}_A(kf_0) = \frac{1}{2}Y\exp[\imath\phi_A(kf_0)]$, $\tilde{Y}_A(-kf_0) = \frac{1}{2}Y\exp[-\imath\phi_A(kf_0)]$. Similar equations hold for $\tilde{Y}_B(nf_0)$. It follows from Eq. (1) that

$$\langle Z(t)\rangle = \frac{1}{2}Y^2\cos[\phi_A(kf_0) - \phi_B(kf_0)]. \tag{3}$$

This quantity is maximal when the phase shifts $\phi_A(kf_0)$ and $\phi_B(kf_0)$ are equal and minimal when they differ by half a cycle.

The decomposition of Eq. (1) is particularly useful in analyzing model behavior under conditions in which the signals $S_A(t)$ and $S_B(t)$ that modulate the bars are sinusoidal (of frequency $f_0 = 1/P$), of equal amplitude $S$, and with phases given by $\phi_A$ and $\phi_B$—as in Experiments 1, 2, and 3. Since each $L_S$ is a linear filter, the outputs of $L_S$, $W_A(t)$ and $W_B(t)$, must be sinusoidal, and their phase difference $\Delta\phi$ must equal the phase difference of $S_A(t)$ and $S_B(t)$, namely $\phi_A - \phi_B$.

### 4.3. The shape of the nonlinearity

The qualitative features of the responses to sinusoidally modulated bars allow us to constrain the possibilities for the nonlinearity $N_S$, the next component of the model. We consider three cases: (i) $N_S$ is trivial (i.e.

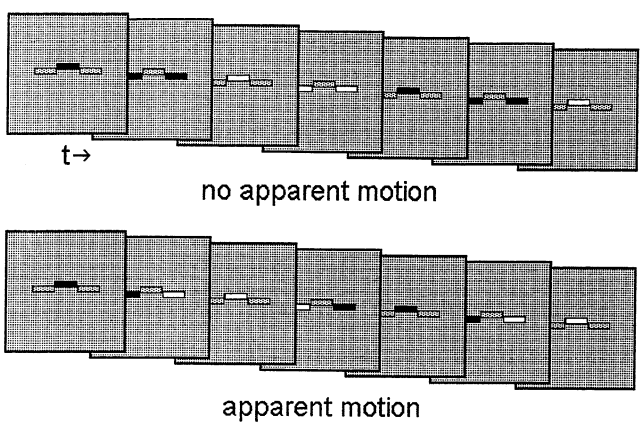


Fig. 10. A spatiotemporal diagram of the visual stimuli used in the apparent motion experiment (Experiment 4). Each frame represents a snapshot of the stimulus at quarter-cycle intervals. Bars were modulated sinusoidally in time. In the 'no apparent motion' condition, the flanking bars were modulated synchronously, with a temporal phase that lagged the central bar (in this example, by 0.25 cycle). In the 'apparent motion' condition, the temporal phase shift between the flanking bars and the central bars was identical, except that one of the flanking bars (the one on the right) led the central bar in phase, while the other flanking bar lagged the central bar in phase.

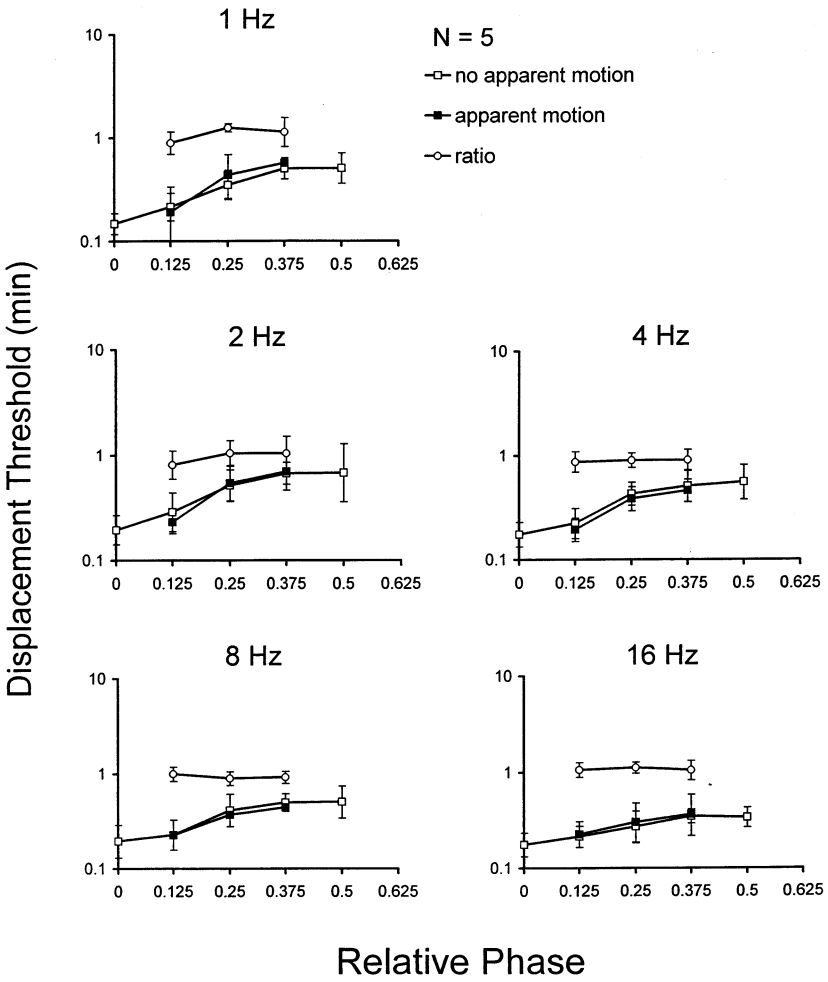


Fig. 11. Cross-subject averages of vernier thresholds as a function of temporal frequency (panel), relative phase, and the presence or absence of apparent motion (open circles: phase shifts not consistent with apparent motion; filled symbols: staggered phases, consistent with apparent motion). Contrast was set to 8 × detection threshold at each temporal frequency. Each data point represents an average of five subjects. Error bars represent ±2 S.E.M. as calculated across subjects, as in Fig. 3.

it can be removed from the model); (ii) $N_S$ has the 'scaling property' (i.e. multiplying its input by a constant positive factor results in multiplying its output by the same factor); and (iii) $N_S$ is a nonlinearity that robustly violates the scaling property. We will show that the results of Experiment 1 are inconsistent with alternatives (i) and (iii), but not (ii).

If the nonlinearity $N_S$ is removed from the model, then the signals $X_A(t)$ and $X_B(t)$ at its output must also be equal-amplitude sinusoids at the input frequency $f_0$, and have a phase difference $\Delta\phi(f_0) = \phi_A(f_0) - \phi_B(f_0)$. Since $L_1$ and $L_2$ are also linear filters, the signals $Y_A(t)$ and $Y_B(t)$ presented to the cross-correlator $N_C$ also must have these characteristics. The amplitudes $Y$ of these sinusoids are determined by the amplitude $S$ of the input, and the characteristics of the filters $L_S$, $L_1$, and $L_2$:

$$Y = S|\tilde{L}_S(f_0)||\tilde{L}_1(f_0)||\tilde{L}_2(f_0)|, \quad (4)$$

where $\tilde{L}_S(f_0)$, $\tilde{L}_1(f_0)$, and $\tilde{L}_2(f_0)$ are the transfer functions of these filters at the input frequency $f_0$. This equation for the amplitudes of the inputs to the cross-correlator, along with Eq. (3), determines the average output of the model $\langle Z(t)\rangle$, assumed to govern the sensitivity to vernier displacement:

$$\langle Z(t)\rangle = \frac{1}{2}S^2|\tilde{L}_S(f_0)|^2|\tilde{L}_1(f_0)|^2|\tilde{L}_2(f_0)|^2 \cos[\Delta\phi(f_0)]. \quad (5)$$

Eq. (5) makes a straightforward prediction: phase-dependence of $\langle Z(t)\rangle$ is determined by the product of frequency-dependent components of the model and the stimulus amplitude $S$. That is, as the input temporal frequency $f_0$ is varied, it should be possible to neutralize any change in phase-dependence (due to effects of the linear filters) by a change in stimulus amplitude $S$ that keeps the product $S|\tilde{L}_S(f_0)\tilde{L}_1(f_0)\tilde{L}_2(f_0)|$ constant. But this is precisely the opposite of what we find: at low

temporal frequencies, there is a marked phase-sensitivity (Figs. 4 and 5), while at high temporal frequencies there is none, and this holds over a wide range of stimulus amplitudes (Figs. 2 and 3).

Eq. (5) states that for a fixed phase offset, $\langle Z(t)\rangle$ increases quadratically with stimulus amplitude $S$, but there is no comparable change in displacement threshold experimentally (Figs. 2 and 3). There are at least two reasonable explanations for this discrepancy. (i) Sensitivity may be a highly saturating function of $\langle Z(t)\rangle$. (ii) Contrast normalization (Heeger, 1992) may intervene at one or more points in the proposed model. However, neither of these possibilities can account for the shift from phase-sensitivity at low frequencies to phase-insensitivity at high frequencies. Thus, we are forced to consider more elaborate models, in which there is a nonlinearity $N_S$ preceding the cross-correlation stage (cases (ii) and (iii) above).

In case (ii), the nonlinearity $N_S$ is assumed to have the 'scaling' property: multiplying its input by a constant positive factor results in multiplication of the output by the same constant factor. Such nonlinearities are described by $X(t) = N_S(W(t))$, where $W(t)$ indicates

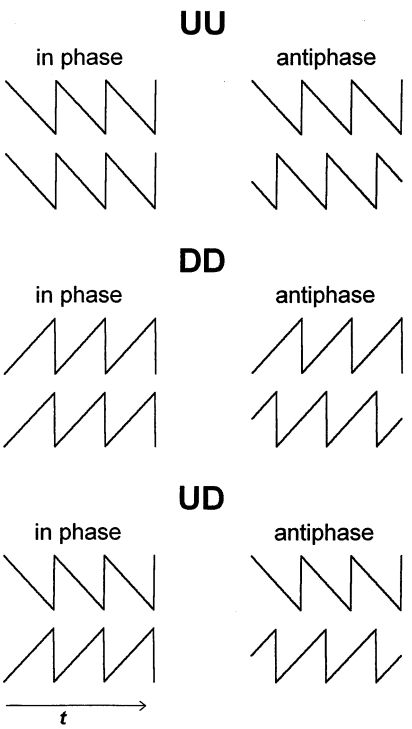


Fig. 12. The temporal modulation signals used in Experiment 5. All waveforms have a mean equal to zero (the background luminance). 'UU' denotes a stimulus configuration in which the waveforms for the two bars both had up-transients. 'DD' denotes a stimulus configuration in which the waveforms for the two bars both had down-transients. 'UD' denotes a stimulus configuration in which one waveform had an up-transient and the other had a down-transient. For each of these three possibilities, waveforms were presented either with synchronous transients ('in phase') or transients separated by, half a cycle ('antiphase').

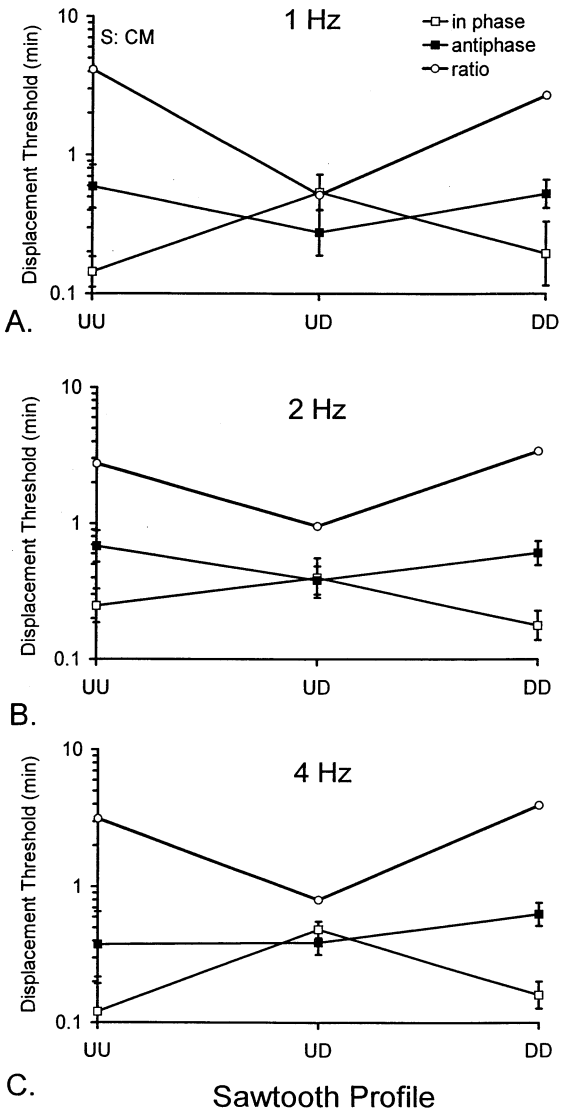


Fig. 13. Vernier thresholds as a function of temporal frequency (panel). sawtooth profile configuration (abscissae), and relative phase of the transient (open symbols: in phase; filled symbols: antiphase). The temporal waveforms are diagrammed in Fig. 12. Contrast was set to 16× detection threshold, determined separately for each frequency and averaged across sawtooth polarity. Other details as in Fig. 2. Subject CM.

the nonlinearity's input at time $t$, $X(t)$ indicates its output and $N_S(w)$ has the form

$$N_S(w) = g_{pos}w, \quad w \geq 0; \quad N_S(w) = g_{neg}w, \quad w \leq 0. \qquad (6)$$

We can assume that $g_{pos} = 1$, by absorbing any overall multiplicative factor into the preceding linear filter. Examples of such nonlinearities include the half-wave rectifier ($g_{pos} = 1, g_{neg} = 0$) and the full-wave rectifier ($g_{pos} = 1, g_{neg} = -1$). This class does not include nonlinearities with a threshold set above zero, since they produce no output for small inputs, but a nonzero output for large inputs. Nonlinearities that satisfy the scaling property can distort a sinusoidal input into a

non-sinusoidal output but the shape of the distorted waveform will be independent of the amplitude of the input. This distortion can be summarized by the Fourier decomposition of its response to a sinusoid (Bedrosian & Rice, 1971). For an input signal $W(t) = W\cos[2\pi f_0 t + \phi(f_0)]$, the nonlinearity's output is given by

$$X(t) = W\sum_{n=0}^{\infty} c_n \cos[2\pi n f_0 t + n\phi(f_0)], \qquad (7)$$

where the coefficients $c_n$ depend only on $g_{neg}$.

Eq. (7) indicates that the signals $X_A(t)$ and $X_B(t)$ at the nonlinearity's output contain sinusoidal components not just at the input frequency (corresponding to $n = \pm 1$ in Eq. (7)), but also a DC component (corresponding to $n = 0$ in Eq. (7)) as well as components at higher harmonics (corresponding to $n = \pm 2, \pm 3, \ldots$). The sizes of these components are determined by the coefficients $c_n$. Since the nonlinearity acts pointwise in time (Eq. (6)), the sizes of these components are independent of the fundamental frequency $f_0$. The other important feature of the coefficients $c_n$ for our analysis is that they decline rapidly as a function of $n$. For the nonlinearity of Eq. (6) the values of $c_n$ (obtained by Fourier transformation of $N_s(\cos(2\pi f_0 t))$ with respect to the period $P = 1/f_0$ are:

$$c_0 = \frac{g_{pos} - g_{neg}}{\pi}; \quad c_1 = \frac{g_{pos} + g_{neg}}{2};$$

$$c_n = 2\frac{g_{pos} - g_{neg}}{\pi}\frac{(-1)^{n/2-1}}{n^2-1} \quad (n > 0, \quad \text{even});$$

$$c_n = 0, \quad \text{otherwise.} \qquad (8)$$

Note that $c_2$ and $c_0$ are comparable ($c_2/c_0 \cong 0.67$), but $|c_4/c_0| \cong 0.13$ and $|c_6/c_0| \cong 0.06$.

According to the decomposition of Eq. (1), each harmonic $nf_0$ in $Y_A(t)$ and $Y_B(t)$ contributes independently to $\langle Z(t)\rangle$, where the contribution of each harmonic is determined by Eq. (3). The signals $Y_A(t)$ and $Y_B(t)$ are derived from $X_A(t)$ and $X_B(t)$ by the successive action of the linear filters $L_1$ and $L_2$. Thus, the amplitudes of their Fourier components at the frequency $nf_0$ are equal to the amplitudes of the corresponding Fourier components of $X_A(t)$ and $X_B(t)$, multiplied by $|\tilde{L}_1(nf_0)||\tilde{L}_2(nf_0)|$. According to Eq. (7), the Fourier components in $X_A(t)$ and $X_B(t)$ at the frequency $nf_0$ have an amplitude $c_n S|\tilde{L}_S(f_0)|$. Finally, the phase shift associated with the $n$th harmonic is $n$ times the phase shift associated with the fundamental, i.e. $\Delta\phi(nf_0) = n\Delta\phi(f_0)$. Thus, for a model that includes a sealing nonlinearity at $N_S$, $\langle Z(t)\rangle$ is given by:

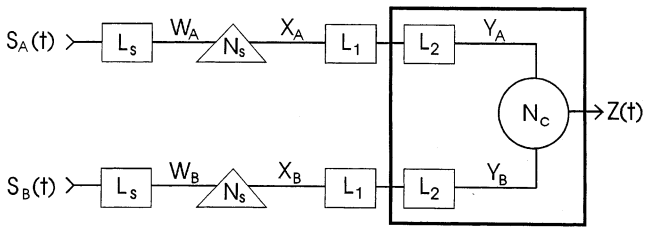


Fig. 15. A model framework for the analysis of the dynamics of vernier acuity, consisting of a stage of independent processing ($L_S$, $N_S$, and $L_1$) followed by a stage of joint processing ($L_2$ and $N_C$). $S_A(t)$ and $S_B(t)$ are the contrasts of the two bars. They are processed separately by identical linear filters $L_S$, and the resulting signals [$W_A(t)$ and $W_B(t)$] are the inputs to a static nonlinearity $N_S$. The outputs $X_A(t)$ and $X_B(t)$ of the separate nonlinear stages $N_S$ are linearly filtered by $L_1$ (within the stage of independent processing) and then $L_2$ (within the stage of joint processing), to form signals $Y_A(t)$ and $Y_B(t)$. These signals are merged by a final nonlinearity $N_C$, akin to a cross-correlator. Sensitivity to displacement is assumed to be monotonically related to the time-average output of $N_C$, denoted $\langle Z(t)\rangle$.

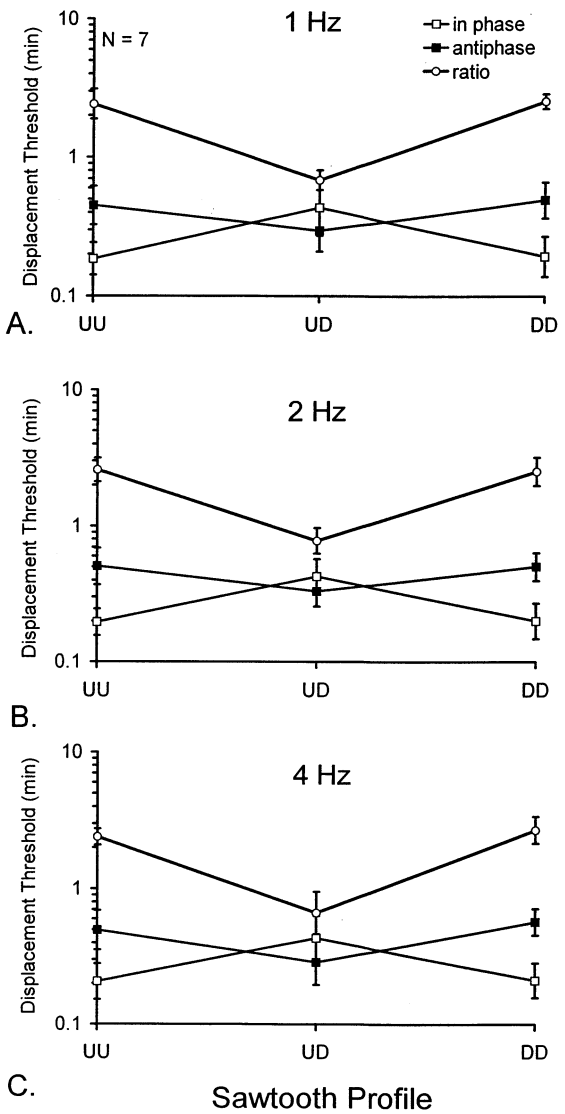


Fig. 14. Cross-subject averages of vernier thresholds as a function of temporal frequency, sawtooth profile configuration, and relative phase of the transient. Each data point represents an average of seven subjects. Error bars represent $\pm 2$ S.E.M. as calculated across subjects. as in Fig. 3. Other details as in Fig. 13.

$$\langle Z(t)\rangle = S^2|\tilde{L}_s(f_0)|^2\left\{c_0^2\,|\tilde{L}_1(0)|^2|\tilde{L}_2(0)|^2 + \frac{1}{2}\sum_{n=1}^{\infty} c_n^2|\tilde{L}_1(nf_0)|^2|\tilde{L}_2(nf_0)|^2\cos[n\Delta\phi(f_0)]\right\}. \quad (9)$$

As in the discussion of Eq. (5), we focus on the phase-dependence of Eq. (9), rather than its overall size as a function of stimulus amplitude $S$ or frequency $f_0$. The first term in this expression is independent of phase. The second term (the sum over the $n$th harmonics) contains all of the phase-dependence, and shows that this phase-dependence interacts with the characteristics of $L_1$ and $L_2$. We focus on the in phase ($\Delta\phi(f_0)=0$) and antiphase ($\Delta\phi(f_0)=\pi$) conditions. Restricted to these two phases, the even-harmonic summands have identical values. Furthermore for nonlinearities of the form (6), the only nonzero odd-harmonic coefficient $c_n$ is $c_1$, since the nonlinearity of Eq. (6) is a sum of a linear component $\frac{1}{2}(g_{pos}+g_{neg})W(t)$ and an even-symmetric component $\frac{1}{2}(g_{pos}-g_{neg})|W(t)|$. We express the phase-dependence component of $Z_{mean}=\langle Z(t)\rangle$ as a kind of Michelson contrast, with $Z_{mean}(f_0, 0)$ denoting its in phase value and $Z_{mean}(f_0, \pi)$ denoting its antiphase value:

$$\frac{Z_{mean}(f_0,0)-Z_{mean}(f_0,\pi)}{Z_{mean}(f_0,0)+Z_{mean}(f_0,\pi)} = \frac{\frac{1}{2}c_1^2|\tilde{L}_1(f_0)|^2|\tilde{L}_2(f_0)|^2}{c_0^2|\tilde{L}_1(0)|^2|\tilde{L}_2(0)|^2+\frac{1}{2}\sum_{n=2,4,6,\ldots} c_n^2|\tilde{L}_1(nf_0)|^2|\tilde{L}_2(nf_0)|^2}. \quad (10)$$

As Eq. (8) shows, the size of the coefficients $c_n$ declines rapidly for $n\geq 4$. If only $c_0$ and $c_1$ were nonzero, then Eq. (10) would indicate that phase sensitivity at the frequency $f_0$ is determined by the transfer functions of $L_1$ and $L_2$ at this frequency. To account for our findings, this would imply that the combined behavior of these filters is bandpass, i.e. that the product $|\tilde{L}_1(f_0)||\tilde{L}_2(f_0)|$ has a maximum near 2 Hz, and sharply declines above 8 Hz. Because of this decline, even though higher even-order coefficients $c_2, c_4,\ldots$ for nonlinearities of the form (6) are nonzero, they will have little influence on the qualitative behavior of Eq. (10), since the contribution of $c_n$ to the denominator of Eq. (10) is multiplied by terms like $|\tilde{L}_1(nf_0)|^2|\tilde{L}_2(nf_0)|^2$. Thus, we conclude that a bandpass characteristic for the combined transfer functions $L_1$ and $L_2$, along with a nonlinearity of the form (6), can account for a phase sensitivity that has the observed frequency- and contrast-dependence. The frequency-dependence of phase sensitivity is approximately given by the product $|\tilde{L}_1(f_0)||\tilde{L}_2(f_0)|$. The main correction to this approximation is due to the denominator term $c_2^2|\tilde{L}_1(2f_0)|^2|\tilde{L}_2(2f_0)|^2$, whose net effect is to blunt phase sensitivity at sufficiently low frequencies ($f_0(\leq 4$ Hz). Note however that the rectification at $N_S$ must be only partial. If $N_S$ were a full-wave rectifier, the decomposition of the output signal $X(t)$ in Eq. (7) would contain only even-harmonic terms. Thus, for a full-wave rectifier, $c_1=0$, and Eq. (10) would predict that the in phase and antiphase conditions would not differ in displacement threshold—contrary to our findings.

This analysis readily extends to case (iii): nonlinearities $N_S$ whose input-output relationship does not have the scaling property. For such nonlinearities, the relative sizes of the coefficients $c_0, c_1,\ldots$ in Eq. (7) depend on the input amplitude $W$, and hence, are contrast-dependent. This contrast-dependence would carry through to Eq. (10), and thus, predict that (at any given frequency) the phase-sensitivity is contrast-dependent. No such dependence is observed experimentally (Fig. 3), so we conclude that a functional model of the dynamics of the vernier signal need not consider nonlinearities that substantially violate the scaling property.

### 4.4. Predictions for quadrature phase

We next extend the analysis of Eq. (9) to the quadrature phase condition to derive additional aspects of the qualitative behavior of the model. The terms in Eq. (9) for $n=2, 6, 10,\ldots$ contribute to the difference in responses between the quadrature condition and the in phase condition, but not to the difference in responses to the in phase and antiphase conditions, since $\cos(\Delta\phi(f_0))=-1$ for the quadrature condition ($\Delta\phi(f_0)=\pi/2$), but 1 for either the in phase ($\Delta\phi(f_0)=0$) or antiphase ($\Delta\phi(f_0)=\pi$) conditions. We use Eq. (9) to calculate and compare responses in these three conditions:

$$Z_{mean}(f_0,0)-Z_{mean}(f_0,\pi/2) = S^2|\tilde{L}_S(f_0)|^2\left\{\frac{1}{2}c_1^2\,|\tilde{L}_1(f_0)|^2|\tilde{L}_2(f_0)|^2 + \sum_{n=2,6,10,\ldots} c_n^2\,|\tilde{L}_1(nf_0)|^2|\tilde{L}_2(nf_0)|^2\right\}, \quad (11)$$

and

$$Z_{mean}(f_0,\pi/2)-Z_{mean}(f_0,\pi) = S^2|\tilde{L}_S(f_0)|^2\left\{\frac{1}{2}c_1^2\,|\tilde{L}_1(f_0)|^2|\tilde{L}_2(f_0)|^2 - \sum_{n=2,6,10,\ldots} c_n^2\,|\tilde{L}_1(nf_0)|^2|\tilde{L}_2(nf_0)|^2\right\}. \quad (12)$$

As shown from the values for $c_n$ provided by Eq. (8), the terms for $n = 6, 10\ldots$ in Eqs. (11) and (12) can be neglected. Thus, were it not for the contribution of $c_2^2|\tilde{L}_1(2f_0)|^2|\tilde{L}_2(2f_0)|^2$, the values of $\langle Z(t)\rangle$ would be equally-spaced for the in phase, quadrature, and antiphase conditions. At low frequencies ($2f_0$ below the cutoff frequency of the combined transfer functions of $L_1$ and $L_2$), this term diminishes the difference between the quadrature phase and antiphase conditions but enhances the difference between the quadrature phase and in phase conditions, consistent with findings in Experiment 3 (Figs. 8B and 9B). If the $c_2$-term dominates the $c_1$-term in Eqs. (11) and (12), then displacement threshold will be higher for quadrature phase than for the antiphase condition. This was not observed experimentally, and, as we will see below, constrains the shape of the nonlinearity $N_S$.

### 4.5. Numerical simulations

We now consider a series of numerical simulations of the model of Fig. 15 for a scaling nonlinearity $N_S$. In these simulations, we focus on matters that could not be settled analytically: the effects of different shapes for the nonlinearity $N_S$; and different kinds of interaction stages $N_C$. All simulations use the same initial filter $L_S$, $L_1$, and $L_2$. As argued above, $L_S$ is irrelevant since it can only produce an overall change in amplitude, and the phase effects are approximately independent of amplitude. The serial combination $L_1$ and $L_2$ are not modelled separately, but rather combined into a single filter $L_C$ whose frequency-dependence is a simple functional form chosen to be a good match for the observed frequency-dependence of phase sensitivity (Figs. 2 and 3), via Eq. (10). Transfer functions of $L_S$ and $L_C$ share the functional form of a bandpass filter,

$$\tilde{L}(f) = \left(\frac{1}{1+\frac{\imath f}{ma}}\right)^m \left(1-\frac{h}{1+\frac{\imath f}{b}}\right) \tag{13}$$

with the following parameters: $m_S = 8$, $a_S = 4\ \mathrm{s}^{-1}$, $h_S = 0.75$, $b_S = 2\ \mathrm{s}^{-1}$; $m_C = 2$, $a_C = 1.5\ \mathrm{s}^{-1}$, $h_C = 0.75$, $b_C = 2.5\ \mathrm{s}^{-1}$. These transfer functions are graphed in Fig. 16.

The model's output $Z_{\mathrm{mean}}(f_0, \Delta\phi) = \langle Z(t)\rangle$ postulated to be monotonically related to psychophysical sensitivity, can be zero or negative for particular choices of frequency $f_0$, relative input phase $\Delta\phi$, $N_S$, and $N_C$. However, psychophysical thresholds exist for all relative phases, and remain reasonably small. In other words, even though there may be no temporal correlation between the modulation profiles of the stimulus components, it is still possible to judge displacement. Thus, there must be some contribution to vernier sensitivity due to mechanisms entirely different in organization from the model of Fig. 15—e.g. positional encoding of extracted features (Burbeck, 1987; Levi & Waugh, 1996). The contribution of this mechanism is denoted $Z_{\mathrm{ext}}$, which is independent both of flicker frequency $f_0$ and relative phase $\Delta\phi$. For simplicity, we assume that these mechanisms are independent, and their contributions add. Thus, to convert $Z_{\mathrm{mean}}(f_0, \Delta\phi)$ into a psychophysical threshold $P(f_0, \Delta\phi)$, we transform it by

$$P(f_0, \Delta\phi) = \frac{1}{Z_{\mathrm{ext}} + \frac{Z_{\mathrm{mean}}(f_0, \Delta\phi)}{Z_{\mathrm{mean}}(f_0, 0)}} \tag{14}$$

The normalization by $Z_{\mathrm{mean}}(f_0, 0)$, which is the maximum value attainable by $Z_{\mathrm{mean}}(f_0, \Delta\phi)$, can be considered as a kind of contrast normalization (Heeger, 1992), since it is the size of a signal generated by a pathway

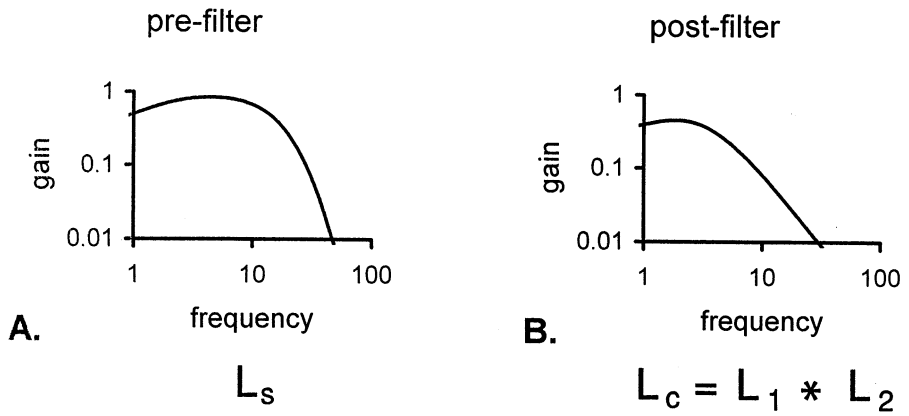


Fig. 16. Panel A: Model transfer function $\tilde{L}_S(f)$ for the linear filter $L_S$ of the separate-processing stage. Panel B: Model transfer function $\tilde{L}_C(f) = \tilde{L}_1(f)\tilde{L}_2(f)$ for the combined effects of linear filters $L_1$ of the separate-processing stage and $L_2$ of the combination stage. These transfer functions share the functional form of Eq. (13), with parameters as given in the text.

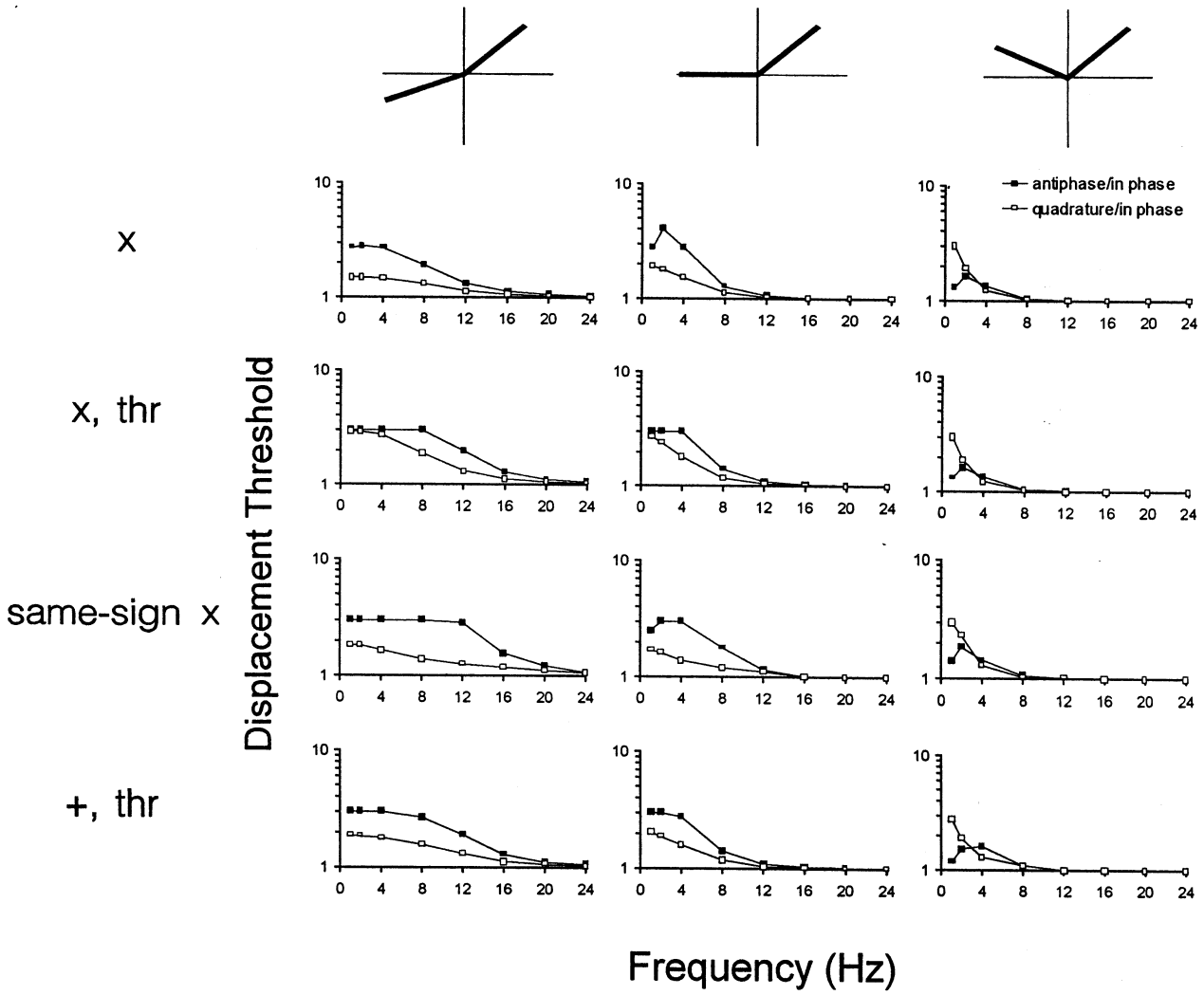


Fig. 17. The dependence of the antiphase/in-phase displacement threshold ratio $P(f_0, \pi)/P(f_0, 0)$ (solid symbols) and the quadrature phase/in-phase sensitivity threshold ratio $P(f_0, \pi/2)/P(f_0, 0)$ (open symbols) for models based on the framework of Fig. 15. Transfer functions $\tilde{L}_S(f)$ and $\tilde{L}_C(f) = \tilde{L}_1(f)\tilde{L}_2(f)$ are shown in Fig. 16. Columns (from left) correspond to choices for the nonlinearity $N_S$: $g_{neg} = 0.5$, $g_{neg} = 0$, and $g_{neg} = -0.5$ in Eq. (6). Rows (from top) correspond to choices for the combination stage $N_C$: multiplication, multiplication followed by threshold. same-sign multiplication, and addition followed by threshold. Values for $Z_{ext}$ in Eq. (14): row 1: 2, 1, 0.3; row 2: 0.5, 0.5, 0.3; row 3: 0.5, 0.5, 0.1; row 4: 0.5, 0.5, 0.05. For further details, see text.

such as Fig. 15 that receives both inputs from the same bar. In the simulations below, as we varied choices of $N_S$ and $N_C$, we chose values of $Z_{ext}$ so that the overall range of variation of $P(f_0, \Delta\phi)$ was about threefold, similar to what we observed. Note that changing the normalization of $Z_{mean}(f_0, \Delta\phi)$. the value of $Z_{ext}$, or the manner in which the contribution of $Z_{ext}$ and $Z_{mean}(f_0, \Delta\phi)$ combine (e.g. including probability summation), would not change the overall dependence of $P(f_0, \Delta\phi)$ on its arguments.

The three columns of Fig. 17 correspond to three choices for the nonlinearity $N_S$. The middle column is a half-wave rectifier ($g_{neg} = 0$ in Eq. (6)); the left and right columns correspond to partial rectification ($g_{neg} = 0.5$) and asymmetric full-wave rectification ($g_{neg} = -0.5$). These choices sample the range between the extremes that we had excluded above: linearity ($g_{neg} = 1$), which predicted no phase-dependence; and full-wave rectification ($g_{neg} = -1$), which predicted that the antiphase and in phase conditions have identical thresholds.

The four rows of Fig. 17 correspond to four choices for the combination stage $N_C$. The first row is straightforward multiplication: $Z(t) = Y_A(t)Y_B(t)$. This corresponds to the combination stage we have considered in the above analytical treatment. Model responses with half-wave rectification ($g_{neg} = 0$, middle graph, first row) are a reasonable match to experimental results for the comparison of antiphase and in phase thresholds (Figs. 3 and 4), and the quadrature phase thresholds are about midway between the antiphase and in phase thresholds. For partial rectification ($g_{neg} = 0.5$, left graph, first row), the predicted frequency-dependence

of the antiphase response is much more gentle than we found experimentally. The blunting of the frequency-dependence for a less severe nonlinearity at $N_S$ is anticipated from our analysis of case (i) above, in which we showed that when the nonlinearity at $N_S$ is removed, frequency-dependence is eliminated. Partial rectification is not ruled out altogether, because the resulting blunting of frequency-dependence can be overcome by sharpening the filter $L_C$ (e.g. by taking $m_C = 8$ in Eq. (13)). For a nonlinearity $N_S$ that approaches full-wave rectification ($g_{neg} = -0.5$, right graph, first row), sharp frequency-dependence is recovered. However, full-wave rectification is inconsistent with the data of Experiment 3 (Figs. 8 and 9), because it predicts that at sufficiently low temporal frequencies, thresholds in the quadrature phase condition are higher than in the antiphase condition. In order for sensitivity to be a monotonic function of phase, as we observed in Experiment 3, $g_{neg}$ must be non-negative. This is because model simulations with negative values of $g_{neg}$ as close to zero as $-0.1$ (not shown) would lead to a noticeable decline in phase-dependence between $\Delta\phi = 3\pi/4$ (0.375 cycles) and $\Delta\phi = \pi$ (antiphase).

The other rows of Fig. 17 correspond to other kinds of interaction. These interaction forms are arguably more physiologically reasonable in that they recognize the existence of thresholds, but are more difficult to treat analytically. The second row postulates a combination stage in which the inputs are multiplied but then subjected to a threshold at 0, to ensure that the combination signal is not negative: $Z(t) = \max\{0, Y_A(t)Y_B(t)\}$. The third row is a modified multiplication stage, in which the inputs only interact when tines are of like sign: $Z(t) = \max\{0, Y_A(t)\}\max\{0, Y_B(t)\} + \max\{0, -Y_A(t)\}\max\{0, -Y_A(t)\}$. The fourth row is summation followed by a threshold, $Z(t) = \max\{0, -Y_A(t) + Y_B(t) - h\}$, where the threshold $h$ is chosen to be a fixed multiple (0.2) of the root-mean-squared value of the inputs to $N_C$. While there are some differences in the details of the predictions (e.g. quadrature phase and antiphase responses at low frequencies are more similar when a threshold is added to the combination stage, as in row 2), the overall features seen with a strict product interaction (row 1) are preserved. There are only very minor differences between crosscorrelation via multiplication (row 1) and crosscorrelation via addition and threshold (row 4), and these can readily be overshadowed by changes in $L_C$. Thus, we conclude that the results of the studies with sinusoidal stimulation are consistent with the model of Fig. 15, provided that the combined effects of $L_1$ and $L_2$ are bandpass (as in Fig. 16), and the nonlinearity $N_C$ is partial or half-wave rectification. The predictions for responses to sinusoidal inputs are independent of $L_S$, and largely independent of $N_C$.

### 4.6. Implications of the sawtooth experiments

The motivation for the experiment based on sawtooth waveforms (Experiment 5) was a qualitative one: since waveforms with rising and falling transients preferentially stimulate ON- and OFF-pathways respectively (Krauskopf, 1980), they provided a means to determine whether the loss of sensitivity to antiphase stimuli was due to processing of the light and dark phases along non-interacting pathways. Additionally, Bowen, Pokorny, and Smith (1989) showed differential sensitivity to detection of a flickering spot modulated by these waveforms (lower thresholds for off-transients), and differential effects of mean illuminance (Bowen, Pokorny, Smith, & Fowler, 1992), providing additional evidence that these stimuli drive ON- and OFF-pathways selectively to at least some extent. Since we found (Figs. 13 and 14) that thresholds for opposite-polarity sawtooth stimuli were lower than thresholds for same-polarity sawtooth stimuli when transients were out of phase, we concluded that stimulus dynamics, not the ON–OFF distinction, played the major role.

Fig. 18 shows model predictions for this experiment, with the same choices for the rectification $N_S$ and the interaction stage $N_C$ that were used in Fig. 17. A frequency of 1 Hz was used for these simulations, but similar results were obtained at 2 and 4 Hz. At 8 Hz and above, the effect of phase and sawtooth polarity was markedly blunted, consistent with the findings of Fig. 17. The reversal of the phase effect for opposite-polarity stimuli is seen for partial rectification ($g_{neg} = 0.5$, left column of Fig. 18) and for halfwave rectification ($g_{neg} = 0$, middle column of Fig. 18), but not for a nonlinearity that approaches full-wave rectification ($g_{neg} = -0.5$, right column of Fig. 18). This (and further simulations with intermediate values of $g_{neg}$) provides additional evidence against nonlinearities that are non-monotonic, independent of the nature of the combination stage $N_C$.

Models with partial- and half-wave rectification are also consistent with the experimental finding (Figs. 13 and 14) that polarity effects are less marked in the antiphase condition than in the in phase condition. Another qualitative feature of the experimental results is that the antiphase thresholds for like-polarity sawtooth stimuli are slightly higher than the in phase thresholds for any sawtooth polarity. This is inconsistent with partial rectification and most kinds of interaction stages (left column of Fig. 18), and thus argues somewhat in favor of half-wave rectification at $N_S$.

Note that for some of the combinations of $N_S$ and $N_C$ in Fig. 18 (particularly addition followed by threshold, bottom row), there is a difference in the predicted thresholds for stimuli in which both components are modulated by antiphase UU and DD saw-

tooth conditions. This difference is a consequence of the asymmetry of the rectification at $N_S$. Although this difference was not observed experimentally, it is not necessarily a reason to discard these candidate models entirely. Even with these choices of $N_S$ and $N_C$, our data could be explained by a pair of the computational units shown in Fig. 15, one of which contains a nonlinearity $N_S$ with an input-output relationship as described by Eq. (6), and one of which contains a nonlinearity that is reversed in polarity:

$$N_S(w) = -g_{pos}w, \quad w \le 0; \quad N_S(w) = -g_{neg}w, \quad w \ge 0. \tag{15}$$

Inclusion of a second pathway of this sort would symmetrize the simulated antiphase responses shown in Fig. 18 and have no effect on the simulated responses shown in Fig. 17.

The sawtooth experiments help to refine the model in another way. The Fourier decomposition of the up- and down-transient sawtooth waveforms have identical amplitudes, but differ in the relative phase of their odd and even harmonics. Thus, in order for the responses to sawtooth waveforms to differ substantially from the responses to sinusoids, components at both the fundamental frequency $f_0$ and the second-harmonic frequency $2f_0$ must pass through the initial filter $L_S$. Otherwise, inversion of the polarity of a sawtooth waveform would have the same effect as a phase shift of half a cycle. As seen in Figs. 13 and 14, these manipulations have different effects, at frequencies up to 4 Hz. Pilot experiments showed that there is no difference at 8 Hz. Thus, we conclude that the linear filter $L_S$ must pass frequencies at least as high as 8 Hz, but attenuate at 16 Hz or beyond, as illustrated in Fig. 16.

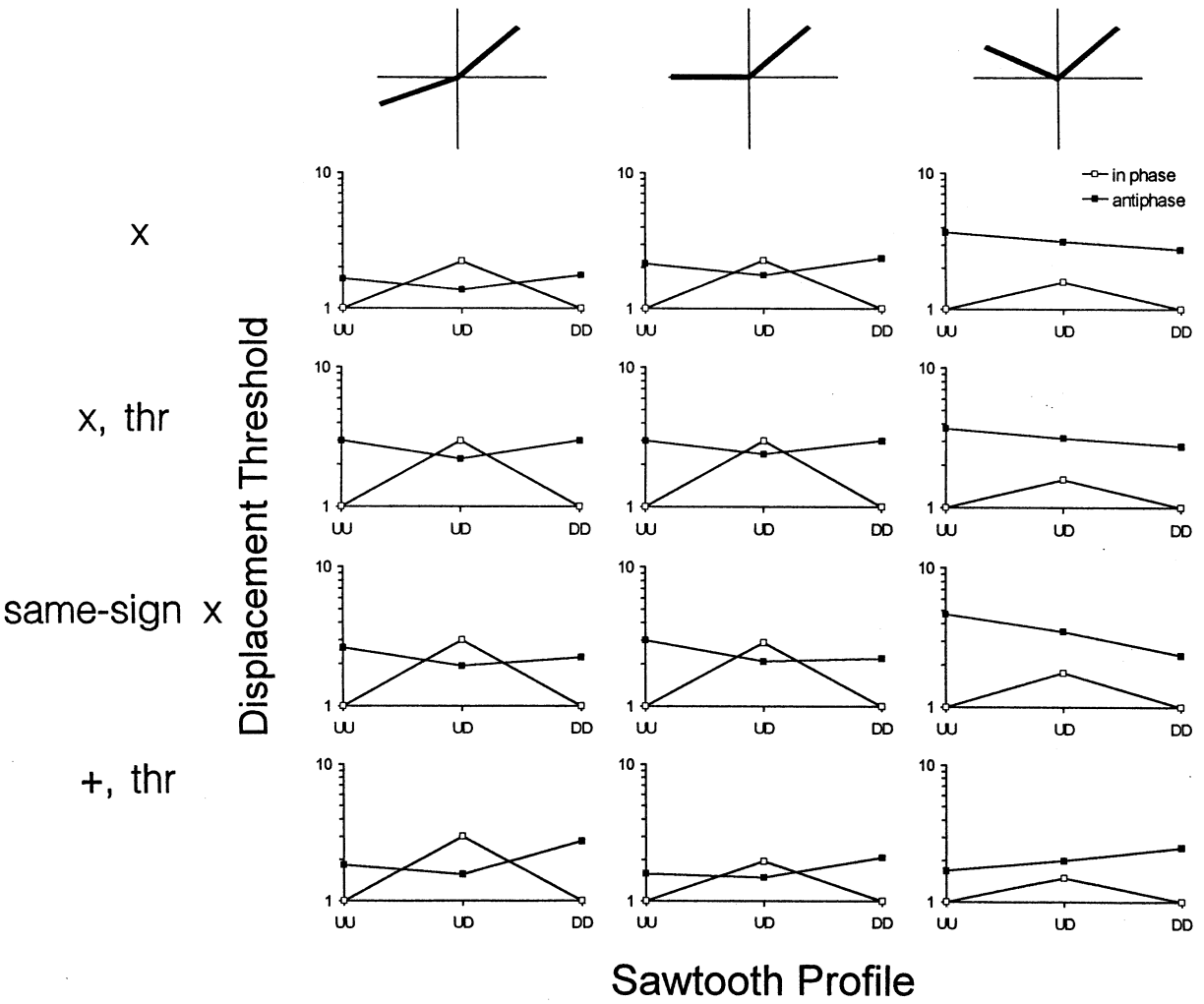


Fig. 18. Predictions of displacement thresholds for sawtooth experiments at 1 Hz, for models based on the framework of Fig. 15. Open symbols: in phase condition. Filled symbols: antiphase condition. Choices for the nonlinearity $N_S$ (columns), the interaction stage $N_C$ (rows), transfer functions $\tilde{L}_S(f)$ and $\tilde{L}_C(f) = \tilde{L}_1(f)\tilde{L}_2(f)$, and $Z_{ext}$ as in Fig. 17.

### 4.7. Relation to previous psychophysical studies

Our analysis has allowed us to distinguish between whether the effects of contrast polarity simply represents the low-frequency limit of asynchronous inputs, or rather reflects separate processing along ON and OFF (Zemon, Gordon, & Welch, 1988; Schiller, 1992) pathways. Transient-stimulus analysis (Wehrhahn & Westheimer, 1993; Beard & Levi, 1997) showed that impairment in performance for asynchronous stimuli was not due to ON versus OFF antagonism, but these studies did not address the possible role of separate ON and OFF signals in the degradation in performance seen when stimuli are presented synchronously, but with opposite polarity. Our work indicates that the degradation in performance under those conditions is not due to separate ON and OFF pathways per se, but to differences in dynamics—the opposite-polarity effect can be reversed by manipulation of stimulus waveforms, as shown in Experiment 5.

Our data are in accord with the view that stimulus components of opposite polarity are jointly processed (Cavanagh, Brussell, & Stober, 1981). However, for stimuli which are spatially complex or changing in time, 'light' and 'dark' are not synonymous with signals along the ON and OFF pathways, respectively. Our approach, based on sawtooth waveforms to distinguish between the ON versus OFF dichotomy and temporal asynchrony, clearly shows that stimuli with prominent ON and OFF transients can be combined in a precise hyperacuity judgment, provided that their phases are adjusted so that their temporal correlation is high.

Our proposed model (Fig. 15) of the dynamics involved in the interaction between stimulus components is fundamentally a local filter model, in which we are able to define the nature of nonlinear elements, and their relationship to temporal filtering processes. This model can be thought of as a grafting of specific dynamics and nonlinearities onto the spatial structure of a 'collector mechanism' (Klein & Levi, 1985; Burbeck, 1987; Morgan et al., 1990; Levi & Waugh, 1996).

This model can also be viewed as an extension of our model for local form processing developed from studies of discrimination of isodipole textures (Victor & Conte, 1989, 1991) We showed that a two-stage model, consisting of local subunits followed by a second cooperative nonlinearity was critical to provide selectivity for extended edges. The local subunit nonlinearity of the form-processing model corresponds to $L_S$, $N_S$ and $L_1$ of Fig. 15, while the second nonlinearity (cooperative pooling) corresponds to $L_2$ and $N_C$ In the analysis of form processing, we modeled the cooperative nonlinearity as summation followed by a threshold with a set-point higher than any single input would typically provide. As shown in the last row of Fig. 18, this kind of process could serve equally well as a cross-correlator.

### 4.8. Relationship to physiological studies

Although cortical mechanisms are doubtless involved in the extraction of displacement (Levi, Manny, Klein, & Steinman, 1983), the spatial information needed for these calculations is already present in the retinal output (Shapley & Victor, 1986; Lee, Wehrhahn, Westheimer, & Kremers, 1993). Spatial sampling and contrast sensitivity are equally important in signaling small displacements. Thus, even though the parvocellular neurons provide a denser sampling of space, the magnocellular neurons' higher contrast sensitivity (Shapley & Perry, 1986) makes this population the likely candidate to carry the spatial signals required for vernier acuity (Wachtler, Wehrhahn, & Lee, 1996), at least at low contrast. We have shown that early rectification is required to account for the frequency- and phase-dependence of vernier judgment. This observation, along with the fact that a significant number of magnocellular ganglion cells (Kaplan & Shapley, 1982) share the *Y* cell's physiologic signature of rectifying subunits (Enroth-Cugell & Robson, 1966; Hochstein, & Shapley, 1976), leads us to speculate that rectification within the ganglion cell's receptive field contributes to $N_S$ of our proposed model.

Since detection of vernier displacements can be viewed as an orientation task (Wilson, 1986; Carney, Silverstein, & Klein, 1995), it is natural to attempt to account for psychophysical thresholds for matched-polarity and opposite-polarity vernier stimuli on the basis of orientation tuning curves of cortical neurons for uniform bars and 'compound' bars (Swindale, 1995), composed of two segments of opposite polarity. For simple cells (Swindale, 1995), these stimuli led to equally sharp tuning curves, but the orientation preference peaks for compound bars differed substantially from the orientation preference for uniform bars. The observation of equally sharp orientation tuning curves for compound bars would appear to be at odds with the notion that simple cells could account for the psychophysical finding of reduced sensitivity in the opposite-polarity condition. However, Swindale argued that simple cells might still be responsible for vernier alignment, and that the increased threshold in the opposite-polarity configurations might be due to difficulty in interpreting off-axis signals, rather than in their intrinsic size or reliability.

An alternative view is that complex cells, which (Swindale, 1995) did show a blunted orientation tuning curve for compound bars, play a key role in judgments of alignment. This is more in keeping with our modeling results, which require two stages of nonlinearity. Quantitative study of complex cell receptive fields (Movshon, Thompson, & Tolhurst, 1978; Spitzer & Hochstein, 1985) clearly indicate the presence of nonlinear subunits, which may contribute to both $N_S$ and $N_C$.

Moreover, our analysis of texture responses in cortical neurons (Purpura, Victor, & Katz, 1994) indicates the computational equivalent of two nonlinear stages, particularly in complex cells. The presence of these two stages would allow complex cells to have the same orientation preference for compound bars as for uniform bars, but would also lead to a reduced sensitivity to compound bars as compared with their sensitivity to uniform bars.

## Acknowledgements

We thank Rahil Rahim, Aaron Hoffman, and Jeremy Perlman for their assistance. A portion of this work was presented at the 1996 and 1997 meetings of the Association for Research in Vision and Ophthalmology in Ft. Lauderdale, FL (Hoffman, Conte, & Victor 1996; Victor, Rahim, & Conte, 1997). This work was supported by NIH grant EY7977.

## References

Beard, B. L., & Levi, D. M. (1997). Vernier acuity with non-simultaneous targets: the cortical magnification factor estimated by psychophysics. *Vision Research*, *31*, 325–346.

Bedrosian, E., & Rice, S. O. (1971). The output properties of Volterra systems (nonlinear systems with memory) driven by harmonic and Gaussian inputs. *Proceedings of the IEEE*, *59*, 1688–1707.

Bowen, R. W., Pokorny, J., & Smith, V. C. (1989). Sawtooth contrast sensitivity: decrements have the edge. *Vision Research*, *29*, 1501–1509.

Bowen, R. W., Pokorny, J., Smith, V. C., & Fowler, M. A. (1992). Sawtooth contrast sensitivity: effects of mean illuminance and low temporal frequencies. *Vision Research*, *32*, 1239–1247.

Burbeck, C. A. (1987). Position and spatial frequency in large-scale localization judgments. *Vision Research*, *27*, 417–427.

Carney, T., Silverstein, D. A., & Klein, S. A. (1995). Vernier acuity during image rotation and translation: visual performance limits. *Vision Research*, *35*, 1951–1964.

Cavanagh, P., Brussell, E. M., & Stober, S. R. (1981). Evidence against independent processing of black and white features. *Perception and Psychophysics*, *29*, 423–428.

Enroth-Cugell, C., & Robson, J. G. (1966). The contrast sensitivity of retinal ganglion cells of the cat. *Journal of Physiology*, *187*, 517–552.

Fendick, M. G., & Swindale, N. V. (1994). Vernier acuity for edges defined by flicker. *Vision Research*, *34*, 2717–2726.

Heeger, D. J. (1992). Normalization of cell responses in cat striate cortex. *Visual Neuroscience*, *9*, 181–197.

Hochstein, S., & Shapley, R. M. (1976). Linear and nonlinear spatial subunits in Y cat retinal ganglion cells. *Journal of Physiology*, *262*, 265–284.

Hoffman, A., Conte, M. M., & Victor, J. D. (1996). Variation in vernier acuity sensitivity with temporal frequency and relative temporal phase(supplement). *Investigative Ophthalmology and Visual Science*, *37*, 735.

Kaplan, E., & Shapley, R. M. (1982). X and Y cells in the lateral geniculate nucleus of macaque monkeys. *Journal of Physiology*, *330*, 125–143.

Klein, S. A., & Levi, D. M. (1985). Hyperacuity thresholds of 1 sec: theoretical predictions and empirical validation. *Journal of the Optical Society of America*, *A2*, 1170–1190.

Kooi, F. L., DeValois, R. L., & Switkes, E. (1991). Spatial localization across channels. *Vision Research*, *31*, 1627–1631.

Krauskopf, J. (1980). Discrimination and detection of changes in luminance. *Vision Research*, *20*, 671–677.

Krauskopf, J., & Farell, B. (1991). Vernier acuity: effects of chromatic content, blur, and contrast. *Vision Research*, *31*, 735–749.

Lee, B. B., Wehrhahn, C., Westheimer, G., & Kremers, J. (1993). Macaque ganglion cell responses to stimuli that elicit hyperacuity in man: detection of small displacements. *Journal of Neuroscience*, *13*, 1001–1009.

Levi, D. M., Jiang, B.-C., & Klein, S. A. (1990). Spatial internal discrimination with blurred lines: black and white are separate but not equal at multiple spatial scales. *Vision Research*, *30*, 1735–1750.

Levi, D. M., & Klein, S. A. (1990). Equivalent intrinsic blur in spatial vision. *Vision Research*, *30*, 1971–1993.

Levi, D. M., Klein, S. A., & Aitsebaomo, A. P. (1985). Vernier acuity, crowding, and cortical magnification. *Vision Research*, *25*, 963–977.

Levi, D. M., Manny, R. E., Klein, S., & Steinman, S. B. (1983). Electrophysiological correlates of hyperacuity in the human visual cortex. *Nature*, *306*, 468–470.

Levi, D. M., & Waugh, S. J. (1996). Position acuity with opposite polarity features: evidence for a nonlinear collector mechanism for position acuity? *Vision Research*, *36*, 573–588.

Levi, D. M., & Westheimer, G. (1987). Spatial interval discrimination in the human fovea: what delimits the interval? *Journal of the Optical Society of America*, *A4*, 1304–1313.

Mather, G., & Morgan, M. J. (1986). Irradiation: implications for theories of edge localization. *Vision Research*, *26*, 1007–1015.

Milkman, N., Schick, G., Rossetto, M., Ratliff, F., Shapley, R., & Victor, J. D. (1980). A two-dimensional computer-controlled visual stimulator. *Behavioral Research Methods and Instrumentation*, *12*, 283–292.

Morgan, M. J., & Regan, D. (1987). Opponent model for line interval discrimination: interval and vernier performance compared. *Vision Research*, *27*, 107–118.

Morgan, M. J., Ward, R. M., & Hole, G. J. (1990). Evidence for positional coding in hyperacuity. *Journal of the Optical Society of America*, *A7*, 297–304.

Movshon, J. A., Thompson, I. D., & Tolhurst, D. J. (1978). Receptive field organization of complex cells in the cat's striate cortex. *Journal of Physiology*, *283*, 79–99.

Nakayama, K., & Silverman, G. H. (1985). Detection and discrimination of sinusoidal grating displacements. *Journal of the Optical Society of America*, *A2*, 267–274.

O'Shea, R. P., & Mitchell, D. E. (1990). Vernier acuity with opposite-contrast stimuli. *Perception*, *19*, 207–221.

Purpura, K., Victor, J. D., & Katz, E. (1994). Striate cortex extracts higher-order spatial correlations from visual textures. *Proceedings of the National Academy of Science (USA)*, *91*, 8482–8486.

Schiller, P. H. (1992). The ON and OFF channels of the visual system. *Trends in Neuroscience*, *15*, 86–92.

Shapley, R., & Perry, V. H. (1986). Cat and monkey retinal ganglion cells and their functional roles. *Trends in Neuroscience*, *9*, 229–235.

Shapley, R., & Victor, J. D. (1986). Hyperacuity in cat retinal ganglion cells. *Science*, *231*, 999–1002.

Spitzer, H., & Hochstein, S. (1985). A complex-cell receptive-field model. *Journal of Neurophysiology*, *53*, 1266–1286.

Swindale, N. V. (1995). Responses of neurons in cat striate cortex to vernier offsets in reverse contrast stimuli. *Visual Neuroscience*, *12*, 805–817.

Toet, A., & Koenderink, J. J. (1988). Differential spatial displacement discrimination thresholds for Gabor patches. *Vision Research*, *28*, 133–143.

Toet, A.., van Eekhout, M. P., Simons, H. L. J. J., & Koenderink, J. J. (1987). Scale invariant features of differential spatial displacement discrimination. *Vision Research*, *27*, 441–451.

Victor, J. D., & Conte, M. M. (1989). Cortical interactions in texture processing: scale and dynamics. *Visual Neuroscience*, *2*, 297–313.

Victor, J. D., & Conte, M. M. (1991). Spatial organization of nonlinear interactions in form perception. *Vision Research*, *31*, 1457–1488.

Victor, J. D., Rahim, R., & Conte, M. M. (1997). Sensitivity of vernier acuity to polarity is due to dynamics, not the on-off dichotomy (supplement). *Investigative Ophthalmology and Visual Science*, *38*, 735.

Wachtler, T., Wehrhahn, C., & Lee, B. B. (1996). A simple model of human foveal ganglion cell responses to hyperacuity stimuli. *Journal of Computational Neuroscience*, *1*, 73–82.

Waugh, S. J., & Levi, D. M. (1993a). Visibility, timing, and vernier acuity. *Vision Research*, *33*, 505–526.

Waugh, S. J., & Levi, D. M. (1993b). Visibility, luminance, and vernier acuity. *Vision Research*, *33*, 527–538.

Waugh, S. J., & Levi, D. M. (1993c). Visibility and vernier acuity for separated targets. *Vision Research*, *33*, 539–552.

Wehrhahn, C., & Westheimer, G. (1990). How vernier acuity depends on contrast. *Experimental Brain Research*, *80*, 618–620.

Wehrhahn, C., & Westheimer, G. (1993). Temporal asynchrony interferes with vernier acuity. *Visual Neuroscience*, *10*, 13–19.

Westheimer, G. (1981). Visual hyperacuity. *Progess in Sensory Physiology*, *1*, 1–30.

Westheimer, G., & Hauske, G. (1975). Temporal and spatial interference with vernier acuity. *Vision Research*, *15*, 1137–1141.

Westheimer, G., & McKee, S. (1977). Spatial configurations for visual hyperacuity. *Vision Research*, *17*, 941–947.

Whitaker, D., Mäkelä, P., Rovamo, J., & Latham, K. (1992). The influence of eccentricity on position and movement acuities as revealed by spatial scaling. *Vision Research*, *32*, 1913–1930.

Whitaker, D., Rovamo, J., Macveigh, D., & Mäkelä, P. (1992). Spatial scaling of vernier acuity tasks. *Vision Research*, *32*, 1481–1491.

Wilson, H. R. (1986). Responses of spatial mechanisms can explain hyperacuity. *Vision Research*, *26*, 453–469.

Zemon, V., Gordon, J., & Welch, J. (1988). Asymmetries in ON and OFF visual pathways of humans revealed using contrast-evoked cortical potentials. *Visual Neuroscience*, *1*, 145–150.